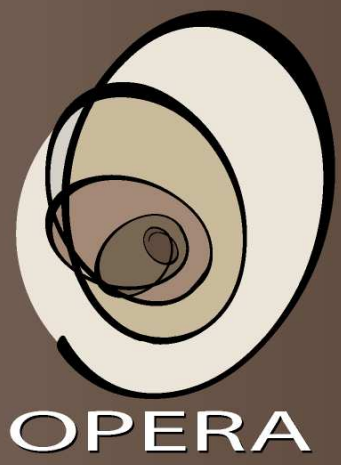

Technical feasibility of a Dutch radioactive waste repository in Boom Clay: Tunnel Crossings

OPERA-PU-TUD321b

Radioactive substances and ionizing radiation are used in medicine, industry, agriculture, research, education and electricity production. This generates radioactive waste. In the Netherlands, this waste is collected, treated and stored by COVRA (Centrale Organisatie Voor Radioactief Afval). After interim storage for a period of at least 100 years radioactive waste is intended for disposal. There is a world-wide scientific and technical consensus that geological disposal represents the safest long-term option for radioactive waste.
Geological disposal is emplacement of radioactive waste in deep underground formations. The goal of geological disposal is long-term isolation of radioactive waste from our living environment in order to avoid exposure of future generations to ionising radiation from the waste. OPERA (OnderzoeksProgramma Eindberging Radioactief Afval) is the Dutch research programme on geological disposal of radioactive waste.
Within OPERA, researchers of different organisations in different areas of expertise will cooperate on the initial, conditional Safety Cases for the host rocks Boom Clay and Zechstein rock salt. As the radioactive waste disposal process in the Netherlands is at an early, conceptual phase and the previous research programme has ended more than a decade ago, in OPERA a first preliminary or initial safety case will be developed to structure the research necessary for the eventual development of a repository in the Netherlands. The safety case is conditional since only the long-term safety of a generic repository will be assessed. OPERA is financed by the Dutch Ministry of Economic Affairs and the public limited liability company Electriciteits-Produktiemaatschappij Zuid-Nederland (EPZ) and coordinated by COVRA. Further details on OPERA and its outcomes can be accessed at `www.covra.nl`.

OPERA-PU-TUD321b
Title: Technical feasibility of a Dutch radioactive waste repository in Boom Clay: Tunnel crossings
Authors: Jiao Yuan, Philip J. Vardon, Michael A. Hicks, Jaap Hart and Peter A. Fokker
Date of publication: June 2017
Keywords: Boom Clay, feasibility, radioactive waste disposal, reliability, tunnel modelling, uncertainty.

TU Delft Delft University of Technology

Technical feasibility of a Dutch radioactive waste repository in Boom Clay: Tunnel crossings

June 2017

Jiao Yuan[1], Philip J. Vardon[1], Michael A. Hicks[1]
Jaap Hart[2] and Peter A. Fokker[3]

[1] Delft University of Technology (TUD), Geo-Engineering Section, Delft
[2] Nuclear Research and consultancy Group (NRG), Petten
[3] Nederlandse Organisatie voor Toegepast Natuurwetenschappelijk Onderzoek (TNO), Utrecht

Contents

Summary

The *Onderzoeks Programma Eindberging Radioactief Afval* (OPERA) is the third national research programme for the geological disposal of radioactive waste in the Netherlands, operating during the period 2011 to 2016. This document reports part of Work Package 3.2.1, where a number of aspects related to the technical feasibility were investigated.

Tunnel linings can be constructed using unreinforced concrete where the stresses acting on them are uniform enough to restrict bending and tension so that they remain under compression. When constructing a series of disposal galleries originating from another gallery, the tunnel lining of the main gallery must be locally removed. In a repository structure, this occurs frequently and therefore it is important to understand whether such technical interventions would compromise the stability of the excavated galleries or whether additional damage is sustained by the clay.

A numerical investigation, using a 3D finite element numerical model (PLAXIS), has been undertaken to investigate the implications of removing (part of) the tunnel lining and installing tunnel crossings. The response of the Boom Clay, in terms of the damaged zone, has been studied, as has the tunnel lining and tunnel crossing and the forces and moments exerted on it. A series of analyses have been undertaken to understand how various aspects impact the behaviour. A parametric study of the critical material model parameters, the initial stress state, the construction methods and the construction sequence is presented.

It is seen in the base case analysis, where the most likely values of properties relevant for these simulations were selected, that the construction of the disposal tunnel had only a limited impact on the damaged zone (plastic and hardening zones) of the Boom Clay around the tunnel. However, the tunnel lining was subjected to significantly increased moments and forces local to the tunnel opening. It was shown that only limited areas should be reinforced, surrounding the tunnel openings, where both tensile stresses and higher than allowable compressive stresses occurred. The majority of the main tunnel and all of the disposal tunnel could remain unreinforced.

The sensitivity analysis provided understanding of the critical properties of the Boom Clay, where the friction angle was seen to be the most important material property, with the in situ stress conditions and construction methods also being important. By adding local support around the tunnel opening during the disposal gallery construction, it was shown that the final maximum moments and maximum forces in the vicinity of the crossings could be lowered, reducing the need for reinforcement.

The results from this study demonstrated that the construction of tunnel openings are technically feasible, without substantially increasing the damage of the surrounding clay or without substantial lining reinforcement. Local reinforcement around the tunnel opening is likely to be required and the construction sequence should be studied in detail prior to construction.

Samenvatting

Onderzoeks Programma Eindberging Radioactief Afval (OPERA) is het derde nationale onderzoeksprogramma naar geologische eindberging in Nederland, uitgevoerd in de periode tussen 2011 tot 2016. Dit document betreft werkpakket 3.2.1, waar een aantal aspecten gerelateerd aan de technische haalbaarheid zijn onderzocht.

Tunnel linings kunnen worden vervaardigd van ongewapend beton indien de krachten op de lining uniform genoeg zijn om buiging en trekkrachten zodanig te beperken dat de lining in het geheel alleen op druk belast wordt. Bij de constructie van een serie bergingsgalerijen vanuit een hoofdgalerij moet de tunnel lining lokaal worden verwijderd. In een eindberging gebeurt dit regelmatig en het is hierom belangrijk begrip te krijgen in mogelijke stabiliteitsproblemen van de galerijen en de extra verstoring van het de omringende kleilaag die zulke technische ingrepen kunnen veroorzaken.

Een numerieke analyse is uitgevoerd met behulp van een 3D numeriek eindige elementen model (PLAXIS), waarmee het effect van het (deels) verwijderen van tunnel lining ten behoeve van het uitbouwen van de hoofdgalerij is onderzocht. Het gedrag van de Boomklei, inzake de verstoringszone, de krachten en momenten op de tunnel lining en op de verbindingssegmenten zijn onderzocht. Een serie analyses is uitgevoerd met als doel de invloed van verscheidende variabelen op het gedrag van de eindberging te begrijpen. Een parametrische studie naar de kritieke modelparameters, initiÃńle spanning, constructiemethoden en constructievolgorde wordt gepresenteerd.

Uit de analyse van de referentiesituatie, waarvoor de meest waarschijnlijke waarden voor relevante materiaaleigenschappen zijn gebruikt, blijkt dat de constructie van de bergingstunnel slechts een beperkte invloed heeft op de verstoringszone (plastische- en hardeningzones) van de boomklei rond de tunnel. Echter, de tunnel lining wordt onderworpen aan significant verhoogde momenten en krachten rond de tunnelopening. De simulaties tonen aan dat slechts enkele plaatsen rond de tunnelopeningen gewapend hoeven te worden. Dit zijn plekken waar zowel trekkrachten als te grote drukkrachten optreden. Het grootste deel van de hoofdtunnel en alle bergingstunnels zouden ongewapend kunnen blijven.

De gevoeligheidsanalyse heeft geleid tot begrip van de kritieke eigenschappen van boomklei; de hoek van inwendige wrijving blijkt de meest belangrijke materiaaleigenschap. Naast de materiaaleigenschappen zijn ook de spanningscondities en de constructiemethoden van belang. Simulaties tonen aan dat door het toevoegen van lokale verstevigingen rond de tunnelopening bij de bouw van eindbergingstunnels, de uiteindelijke maximale momenten en krachten in de nabijheid van de aansluiting verminderd kunnen worden. Hierdoor wordt de noodzaak om te wapenen verminderd.

Het resultaat van dit onderzoek toont aan dat het technische mogelijk is tunnelopeningen te construeren, zonder substantieel de verstoring aan de omliggende kleilaag te vergroten of zonder substantiÃńle verstevigingen aan de tunnel lining. Lokale versteviging rond de tunnelopening is waarschijnlijk nodig en de installatievolgorde dient in detail bestudeerd te worden voorafgaand aan de constructie.

Notation

This list contains definitions of acronyms and symbols including dimensions. All symbols are also defined in the text. The dimensions are defined in typical SI units.

Symbol	Definition	Unit
Acronyms		
HS	Hardening Soil	
NRG	Nuclear Research and consultancy Group (NL)	
OCR	Over-consolidation ratio	
OPERA	Onderzoeks Programma Eindberging Radioactief Afval	
TNO	Nederlandse Organisatie voor Toegepast Natuurwetenschappelijk Onderzoek (NL)	
TUD	Delft University of Technology (NL)	
WP	Work Package	
Greek letters		
γ	Unit weight	[N m^{-3}]
γ'	Effective unit weight	[N m^{-3}]
γ_w	Unit weight of water	[N m^{-3}]
μ	Mean	[-]
ν_l	Lining Poisson's ratio	[-]
ν_{ur}	Unloading-reloading Poisson's ratio	[-]
ϕ'	Effective friction angle	[°]
ψ	Dilation angle	[-]
σ'_{xx}	Horizontal effective stress	[Pa]
σ'_{yy}	Horizontal effective stress	[Pa]
σ'_{zz}	Vertical effective stress	[Pa]
σ_{outer}	Stress at the outer edge of a beam	[Pa]
Latin letters		
A	Cross-sectional area	[m^2]
c'	Effective cohesion	[Pa]
D	Diameter	[m]
d	Depth	[m]
d_l	Lining thickness	[m]
d_{oc}	Overcut thickness	[m]
e	Void ratio	[-]
E^{ref}	Reference moduli used to calculate stress dependent modulus	Pa]
E_l	Lining Young's modulus	[Pa]
E_{50}	Secant modulus	[Pa]
E_{oed}	Oedometer modulus	[Pa]
E_{ur}	Unloading/reloading modulus	Pa]
I	Moment of intertia	[m^4]
K_0	At rest coefficient of lateral earth pressure	[-]
K_0^{NC}	Coefficient of earth pressure at rest for NC conditions	[-]
M	Moment	[N m]
m	HS model exponent	[-]
N	Axial force	[N]

p^{ref}	Reference stress	Pa]
r_c	Cavity radius (external radius)	[m]
X_i	Variable	[-]
y	Distance from the outer edge of the lining to the netrual axis of bending	[m]
$M_{l1,max}$	Maximum longitudinal bending moment in liner per metre	[N]
$M_{l1,min}$	Minimum longitudinal bending moment in liner per metre	[N]
$M_{22,max}$	Maximum hoop bending moment in liner per metre	[N]
$M_{22,min}$	Minimum hoop bending moment in liner per metre	[N]
$N_{l,max}$	Maximum longitudinal axial force in liner per metre	[N m^{-1}]
$N_{l,min}$	Minimum longitudinal axial force in liner per metre	[N m^{-1}]
$N_{2,max}$	Maximum hoop axial force in liner per metre	[N m^{-1}]
$N_{2,min}$	Minimum hoop axial force in liner per metre	[N m^{-1}]
R_f	Failure ratio	[-]
r_{HZ}	Radial extent of the shear hardening zone (HS model)	[m]
r_{PZ}	Radial extent of the plastic failure zone (HS model)	[m]

1 Introduction

This report is part of an investigation into the principle feasibility of a deep geological repository for radioactive waste in the Netherlands. This work is undertaken as part of the *Onderzoeks Programma Eindberging Radioactief Afval* (OPERA) research programme in Work Package (WP) 3.2.1. This report follows from WP 3.1, where a number of additional aspects relating to the principle feasibility were identified for further investigation. The results of WP 3.2.1 are presented in the following reports:

- Yuan, J., Vardon, P.J., Hicks, M.A., Hart, J., Fokker, P.A. (2017) Technical feasibility of a Dutch radioactive waste repository in Boom Clay: Plugs and seals. OPERA-PU-TUD321a.
- Yuan, J., Vardon, P.J., Hicks, M.A., Hart, J., Fokker, P.A. (2017) Technical feasibility of a Dutch radioactive waste repository in Boom Clay: Tunnel crossings. OPERA-PU-TUD321b.
- Vardon, P.J., Buragohain, P., Hicks, M.A., Hart, J., Fokker, P.A., Graham, C.C. (2017) Technical feasibility of a Dutch radioactive waste repository in Boom Clay: Thermo-hydro-mechanical behaviour OPERA-PU-TUD321c.
- Li, Y., Vardon, P.J., Hicks, M.A., Hart, J., Fokker, P.A. (in prep) Technical feasibility of a Dutch radioactive waste repository in Boom Clay: Geomechanical validation. OPERA-PU-TUD321d.

The main objective of this report is to investigate the implications of the construction of tunnel crossings, connecting right-angled galleries and/or disposal sections of the proposed Dutch radioactive waste repository. The research was undertaken by *Delft University of Technology* (TUD), *Nuclear Research and consultancy Group* (NRG) and *Nederlandse Organisatie voor Toegepast Natuurwetenschappelijk Onderzoek* (TNO) during the period from 5-2015 till 6-2016.

1.1 Background

Storage and disposal of radioactive waste in deep geological formations is proposed as the most likely option for the Netherlands and worldwide. Within this concept of a geological disposal system, Boom Clay is considered as a potential host rock in the Netherlands. The repository concept in the Netherlands (Verhoef et al., 2014) consists of a series of disposal galleries which must be excavated from other tunnels (either primary or secondary tunnels). In typical tunnel design, it is not common to have many perpendicular galleries, and therefore engineering over-design may be typical to ensure stability. Moreover, in typical tunnel systems, it is not common to have many parallel tunnels, with perhaps two parallel tunnels being usual.

In Arnold et al. (2015), the mechanical reponse of the excavation of a single tunnel of in Boom Clay and the required spacing between adjacent tunnels were investigated. The results suggested that the tunnel spacing, for mechanical stability, could be reduced. Therefore, the tunnel crossings became more critical to investigate. At tunnel intersections, the symmetry of the stress field will be lost, and therefore the lining at the tunnel crossings will be subjected to bending and torsion stresses. Moreover, the host rock behavior at the intersection is a complex, three-dimensional problem, and therefore requires 3D numerical simuation.

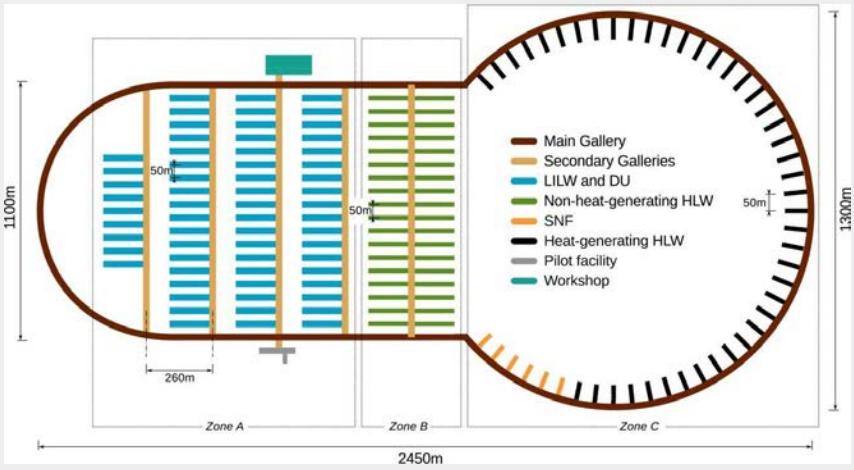

Figure 1.1: Repository layout (after Verhoef et al., 2014).

In the Dutch repository, there are a variety of tunnel crossings (Verhoef et al., 2014) as shown in Figure 1.1 and summarised as:

(i) Shaft and main gallery;

(ii) Main gallery and secondary gallery;

(iii) Main gallery and deposition tunnel;

(iv) Secondary gallery and deposition tunnel.

The most common case is the main or secondary galleries crossing with deposition tunnels. Both, the main and secondary galleries have the same proposed external diameter (4.8 m), with the disposal tunnel proposed to have a smaller external diameter of 3.2 m. Therefore this crossing type is the focus of this report.

Usually in tunnel crossings there is a 'parent' or main tunnel, which is built first and generally has a larger diameter than the 'child' or subsidiary tunnel. The opening for the child tunnel is therefore broken out in the parent tunnel lining. The opening for junctions is carried out from the main (parent) tunnel after the full tunnel profile has been constructed. Support rings may be needed at a sufficient distance (approximately 4-5 tunnel diameters) ahead of the junction to stabilize the main tunnel prior to lateral opening (and to give sufficient working room). Pre-support can be placed before the opening, to redistribute stresses around the opening of the concrete lining. Pre-support can comprise local thickening or reinforcing of the concrete lining.

Most of the previous research on tunnel behaviour was focused on the behaviour of straight tunnels. These studies often focused on the prediction of the ground settlements due to the construction of the tunnels. However, relatively little research on the subject of modelling tunnel crossings has been published. Early research on tunnel crossings was conducted by estimating the stress concentration due to a circular hole in a flat infinite plate using elasticity theory (Hoek and Brown, 1980; Pant, 1971; Riley, 1964; Young, 1989). Later, Takino et al. (1985) investigated the ground movements at the tunnel crossing by considering various rock properties and intersection angles using a 2D numerical model. Biliris and Purwodihardjo (2005) conducted a 2D plane stress numerical analysis to study the lining opening, but ignored the soil-structure interaction and bending moments in the lining. However, the stresses, deformations and plastic behaviour of the soil at tunnel crossings are intrinsically 3D; therefore 2D modelling has distinct disadvantages and may lead to unrealistic and unreliable results, i.e., as reported by Moon and Lee (1991), who found large deviations between 2D and 3D models around tunnel crossings, with 2D modelling overestimating the factor of safety.

As computer power and modelling techniques have developed, 3D analysis was used more widely. Tsuchiyama et al. (1988) investigated the 3D deformation behaviour of the surrounding soils around tunnel crossings, and found that the influence area along the main tunnel was approximately 1-3 tunnel diameters. Thareja et al. (1985) investigated the various rock properties on the displacements and lining stresses at the intersection area using a 3D numerical model. Hafez (1995) investigated the bending moments on tunnel linings by applying pressure on the lining without considering any surrounding soils, with the results indicating that the bending moments on the lining were not negligible and needed to be taken into account in design. Thareja et al. (1997) investigated the construction sequences of a tunnel crossing using shell or solid elements to model the lining, and springs to simulate the soil. Jäger (2002) reported a case study of tunnel crossing design, where a 3D numerical model was used to model the soil and the construction sequences, to improve the design of the tunnel crossing. Ren et al. (2005) studied the stress state in the lining around the tunnel crossing area. Jones (2007) investigated the behaviour of a tunnel crossing by both numerical modelling and in-situ measurements, with the results indicating that 3D modelling and the construction sequence were important factors when modelling tunnel openings. Hsiao et al. (2009) investigated the displacements and plastic zones in the tunnel crossing area by considering various rock properties and intersection angles, and investigated the impact on the type and amount of support at the opening area. Spyridis and Bergmeister (2015) studied the structural response of a parent tunnel when a near-circular breakout was made for a perpendicular child tunnel, although the constitutive behaviour of the soil was highly simplified; it was found that the moments increased significantly, as well as the tension longitudinally. Li et al. (2016) investigated the deformation, stress and plastic zone responses of a tunnel intersection of a subway station using FEM simulations.

For geological disposal in the Netherlands, the depth of tunnels and therefore the in-situ stresses are high compared to other tunnels. Moreover, due to the plastic nature of the Boom Clay, the tunnel lining will experience a radial stress of approximate 2-10 MPa (Arnold et al., 2015). Any signifcant damage to the clay rock may have a number of detrimental effects: (i) to increase locally the permeability, (ii) to increase the loads on the lining, therefore potentially impacting the tunnel stability. The bending moments in the lining are also important, so that any steel reinforcement at the crossing can be assessed. The inclusion of steel is not favourable for the long term performance of the underground repository, due to corosion induced hydrogen production, as the overall hydrogen production rate must be lower than the diffusive capacity of the surrounding clay medium (Van Cotthem et al., 2012).

1.2 Objectives

The objective of this report is to study the effects of a tunnel crossing on the mechanical behaviour of the Boom Clay and the liner stresses in the proposed geological disposal facility, using 3D numerical modelling. This research has focused on the following aspects of tunnel crossing:

(i) To investigate the construction feasibility of the tunnel crossings.

(ii) To study the additional clay plasticity induced by tunnel crossings.

(iii) To study the structural stability of the concrete lining, including additional bending moments and torsion, on the introduction of tunnel crossings.

1.3 Outline of the report

The numerical investigation undertaken is outlined in Chapter 2, with the methodology presented in Section 2.1, and the results given in Section 2.2. The results are discussed in detail, firstly through the base case results in Section 2.2.1, where the impact on the clay damaged zone and the lining are discussed. The results of the sensitivity analysis are given in Section 2.2.2, and the conclusions are summarised in Chapter 3.

2 Numerical investigation

2.1 Methodology

2.1.1 Three dimensional modelling of tunnel crossing

The response of the Boom Clay in the Dutch repository concept, due to the excavation of a tunnel, was investigated numerically in two and three dimensions, utilising the PLAXIS finite element software package, by Arnold et al. (2015). The Hardening Soil (HS) model was employed to describe the mechanical behaviour of the Boom Clay, and sensitivity analyses were performed by varying the HS model parameters, state variables and boundary conditions. The HS model was found by Arnold et al. (2015) to well reproduce the non-linear behaviour of Boom Clay, specifically the change in stifness and the mobilisation of the shear strength; it does not, however, simulate strain softening. In this report, the same strategy has been followed to investigate the response of the Boom Clay due to the construction of tunnel crossings, altgough, due to the intrinsically 3D nature of a tunnel crossing, only 3D models have been used. The finite element software package PLAXIS 3D AE (Plaxis, 2015) has been utilised.

As the most common tunnel crossing (based on diameters), a main/secondary gallery and a disposal drift (HLW gallery) have been modelled. As shown by Jones (2007), the construction sequence is important to simulate, in order to accurately predict the behaviour of the tunnel lining and the host rock. Following the approach taken by Arnold et al. (2015), which has here been extended for tunnel crossings, the following consecutive stages have been simulated:

(i) a K_0 stage, where the initial vertical and horizontal stresses were calculated (shown in Figure 2.1(b));

(ii) a parent tunnel excavation and construction stage, where the tunnel lining was included and contracted to represent rock relaxation (see Figure 2.2(a));

(iii) a tunnel lining removal stage, where the tunnel lining was locally removed (see Figure 2.2(b));

(iv) a child tunnel excavation and construction stage, where the tunnel lining was included and a local rock layer contracted representing rock relaxation (see Figure 2.2(c));

As in Arnold et al. (2015), a depth of $z = 500$ m has been modelled and the HS model used. The model consists of a length of 30 m of the main 'parent' tunnel, with a diameter $D = 4.8$ m and an installed overcut of $d_{oc} = 75$ mm, and a disposal 'child' tunnel with a diameter $D = 3.2$ m and an overcut of $d_{oc} = 75$ mm. The tunnel lining consists of ring-shaped concrete segments, and for the main gallery the lining thickness is 0.55 m and for the disposal tunnel the lining thickness is 0.50 m (Verhoef et al., 2014). After a preliminary study of the boundary effects, the 3D model domain was set up with dimensions of 120 m length in the x-axis direction, 80 m wide in the y-axis direction and 80 m deep in the z direction, with an additional 5 m layer in the K0 stage to determine the initial stresses, as shown in Figure 2.1. These dimensions only represent half of the simulated model due to symmetry in the x-z vertical plane.

In the K_0 stage (i) the initial vertical effective stresses in the domain were calculated based on a hydrostatic water pressure distribution, i.e. $\sigma'_{zz} = (\gamma - \gamma_w)d$ (where γ is the unit weight of the

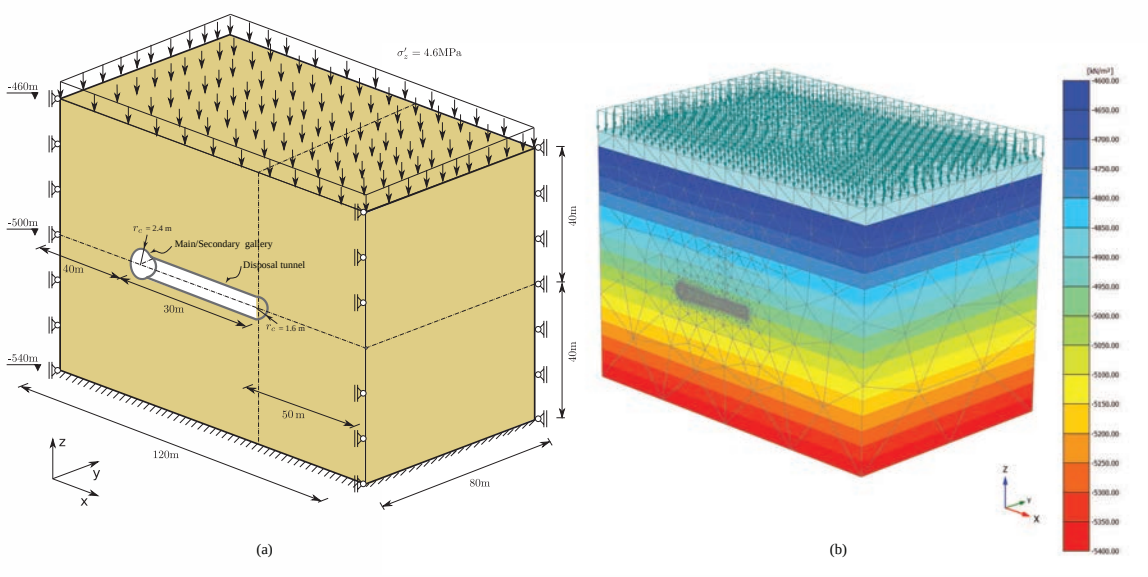

Figure 2.1: Three dimensional excavation of tunnel crossing at 500m depth: (a) model domain; (b) initial effective vertical stresses and discretisation.

soil and γ_w is the unit weight of water). The initial horizontal effective stresses were then computed ($\sigma'_{xx} = \sigma'_{yy} = K_0\sigma'_{zz}$), where K_0 is the coefficient of lateral earth pressure at rest. This procedure takes account of the over-consolidation ratio (OCR) through the chosen value of K_0.

In this model, in contrast to Arnold et al. (2015), the full height of the soil domain is not utilised in the calculation of the initial stresses, due to a limitation in the mesh size generation for the smallest elements (on the tunnel lining). To enable a reduction in the minimum element size, in order to increase the accuracy of the moment calculation, the K_0 model domain is divided into two layers: the upper layer is a so-called heavy layer which is 5 m in depth with an effective soil unit weight of 920 kN/m^3 to represent the full overburden of the soil above -460 m; the second layer is 80 m in depth with an effective soil unit weight of 10 kN/m^3 to represent the Boom Clay (see Figure 2.1(b)). The bottom boundary was fixed both laterally and vertically; the lateral boundaries were fixed in the horizontal direction and free in the vertical direction; and the top boundary was free, equivalent to applying a fixed stress of $\sigma'_{zz} = 4.6$ MPa on the top of the second layer. The spatial discretisation yielded 255,007 ten-node tetrahedral elements with 362,699 nodes, with the mesh shown in Figure 2.1(b).

In phase (ii) the 30 m long main gallery was excavated in the y-direction and the tunnel lining was contracted to simulate the rock relaxation into the overcut. The length was selected so that the tunnel end did not affect the results at the tunnel intersection, and is not the actual length of the tunnel.

In phase (iii) a portion of the main gallery tunnel lining was removed at the location of the tunnel crossing. During the last phase (iv) a 30 m long disposal gallery was excavated in the x-direction. The staged excavation process of the main gallery and disposal tunnel were not considered during the numerical simulation, i.e. all galleries are excavated instantly.

In order to simulate the deformation of the rock due to the overcut, a volumetric strain was applied. In Arnold et al. (2015), this was undertaken by contracting the lining, however in 3D models this was found to yield unrealistic local stresses and moments on the lining. In this work, this was undertaken by applying a predefined volumetric strain on the soil along the lining.

The lining segments of the galleries are modelled by using structural elements, and the interaction between the tunnel lining and the surrounding soil are simulated by using interface elements.

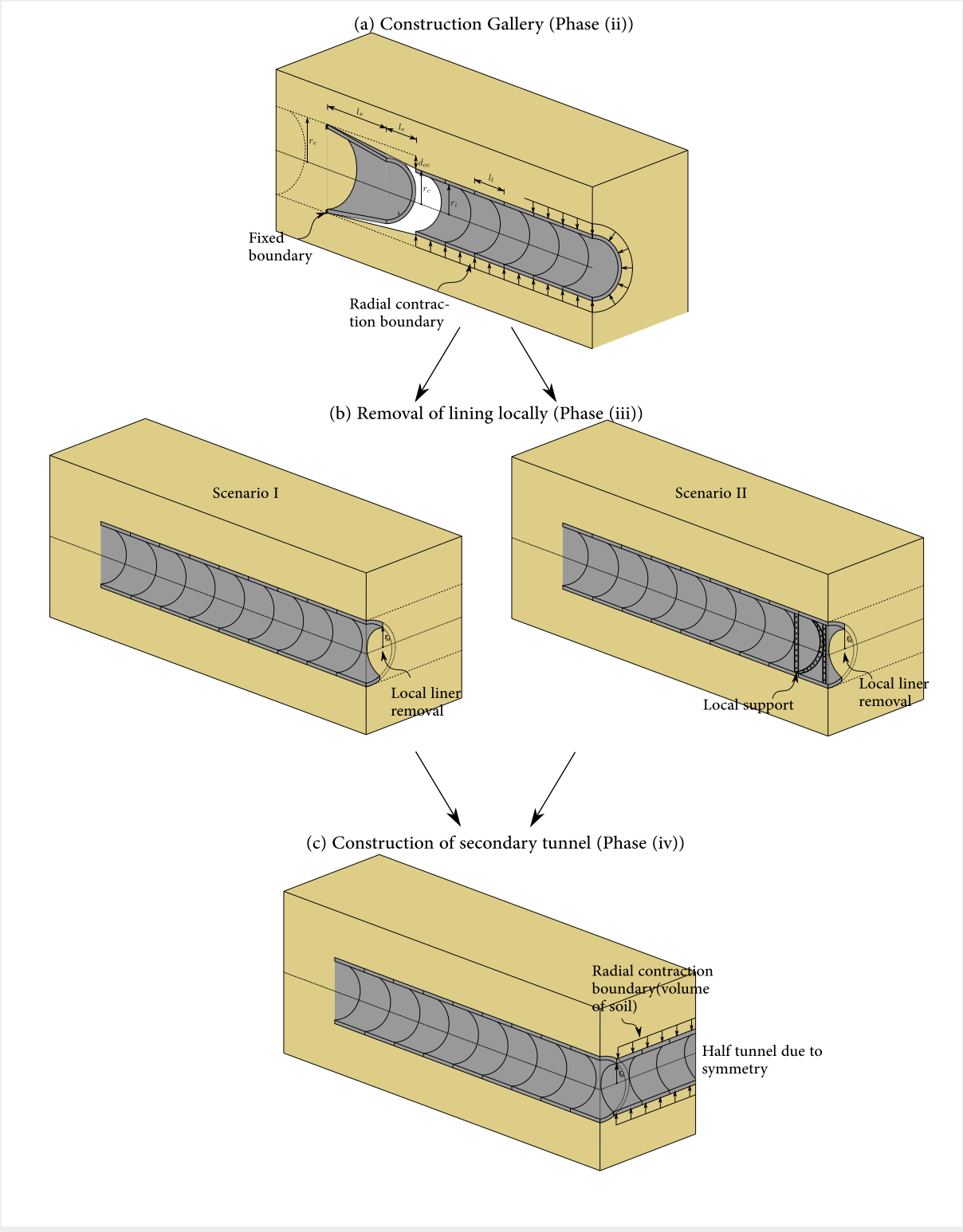

Figure 2.2: The construction model phases for three-dimensional tunnel crossing.

2.1.2 Parameter selection

A review of constitutive modelling of Boom Clay was presented in Arnold et al. (2015). The performance of different material models to simulate Boom Clay behaviour was also assessed, and the results indicated that the HS model was found to perform best. The material response is non-linear elastic inside the yield loci, or linear elastic under triaxial conditions (constant σ_3'). Non-linear elasto-plastic strains induced by shear hardening are primarily controlled by the secant modulus E_{50}, whereas the Oedometer modulus E_{oed} controls the elasto-plastic strains induced due to cap hardening and the Mohr-Coulomb criterion defines failure. The major disadvantage is that strain-softening cannot be simulated. The HS model is one of the advanced soil models implemented in PLAXIS, which is more commonly utilised by geotechnical engineers to compute soil response under compressive loading as well as extensive-shear loading, e.g. due to soil excavation. For more details of the HS model, one can refer to Schanz (1998) and Schanz et al. (1999). The soil parameters used in this research, based on those in Arnold et al. (2015), are given in Table 2.1. Due to the low permeability of Boom Clay and that the immediate response of the lining opening is being considered, undrained analyses have been conducted.

Table 2.1: Boom Clay soil property values and state variables for a mechanical sensitivity analysis to assess a deep tunnel excavation. The parameters, when other parameters vary, are printed in bold.

Variable	X_i	Unit	Lower μ_{X_i}	Midμ_{X_i}	Upper μ_{X_i}
Effective cohesion	c'	[MPa]	0.3	**0.5**	0.7
Effective friction angle	ϕ'	[°]	7.5	**12.5**	17.5
Secant modulus*	E_{50}^{ref}/E_{50}	[MPa]	80/200	**120/300**	160/400
Unloading/reloading modulus*	E_{ur}^{ref}/E_{ur}	[MPa]		**360/900**	
Oedometer modulus **	E_{oed}^{ref}/E_{oed}	[MPa]	80/200	**120/300**	160/400
Unloading/reloading Poisson's ratio	ν_{ur}	[−]		**0.3**	
HS model exponent	m	[−]		**0.8**	
Dilation angle	ψ	[°]		**0.0**	
Earth pressure at rest	K_0	[−]	0.8	0.9	**1.0**
Over-consolidation ratio	OCR	[−]		**2.2**	
Unit weight	γ	[kNm$^-3$]		**20**	
Void ratio	e	[−]		**0.7**	
Reference stress	p^{ref}	[MPa]		**0.1**	
Failure ratio	R_f	[−]		**0.9**	
Earth pressure at rest NC-state	K_0^{NC}	[−]		$1-\sin\phi'$	

* E^{ref} is approximated for E at 500m depth with $\sigma_3' \simeq -5$MPa and $p^{ref} = 0.1$MPa.

** $E_{oed}^{ref} = E_{50}^{ref}$

The tunnel lining property values are summarised in Table 2.2.

2.1.3 Analyses setup and sensitivity analysis

A base case analysis was undertaken, using the parameters given in Table 2.1 in bold, for a repository at 500 m depth and an overcut of 75 mm. For a non-linear 3D analysis, the numerical simulations are computationally expensive, and therefore it is important to reduce the number of parameters used in the sensitivity analysis. Arnold et al. (2015) performed a sensitivity analysis on the response of the Boom Clay due to the excavation, using a 2D plane strain model, by varying the HS model parameters. This analysis evaluated the importance of each unknown parameter with respect to the model response. The results indicated that, for the impact on the extent of the plastic zone and

Table 2.2: Circular concrete lining property values.

Variable	Symbol	Unit	HLW	Main/Secondary/LILW	Shaft
Cavity radius	r_c	[m]	1.6	2.4	3.1
Lining thickness	d_l	[m]	0.5	0.55	0.6
Young's modulus	E_l	[MPa]	35 000	35 000	35 000
Poisson's ratio	ν_l	[−]	0.2	0.2	0.2
Axial stiffness*	$EA^{*}*$	[MN m^{-1}]	17 500	19 250	21 000
Bending stiffness*	EI^{***}	[MN m^2 m^{-1}]	364.58	485.26	630.00

* Properties determined from lining geometry and Young's modulus.

** Cross section area per tunnel lining meter: $A = d$ [m^2 m^{-1}]

*** Second moment of intertia per tunnel lining meter: $I = d^3/12$ [m^4 m^{-1}]

the lining forces, the most sensitive parameters were the effective cohesion (c'), the effective friction angle (ϕ'), the reference secant modulus (E_{50}^{ref}) and the earth pressure coefficient at rest (K_0). Therefore, in this research these four critical parameters have been varied in a sensitivity analysis. In addition, the overcut for the tunnels and the depth were seen, in Arnold et al. (2015), to be critical. Moreover, the local support around the tunnel opening is investigated here.

Four sets of analyses have been performed, as detailed below:

Set A: A sensitivity analysis, which investigates the response of the Boom Clay and the lining to variation in four critical HS model parameters, $\mathbf{X} = \{c', \phi', E_{50}^{ref}, K_0\}$, for a repository at 500 m depth and an overcut of $d_{oc} = 75$mm.

Set B: A sensitivity analysis, again investigating the response of the Boom Clay and the lining to variation in four critical HS model parameters, $\mathbf{X} = \{c', \phi', E_{50}^{ref}, K_0\}$, for a repository at 500 m depth, but increasing the overcut to $d_{oc} = 100$ mm.

Set C: A sensitivity analysis, again investigating the response of the Boom Clay and the lining to variation in four critical HS model parameters, $\mathbf{X} = \{c', \phi', E_{50}^{ref}, K_0\}$, with a repository at 700 m depth and an overcut of $d_{oc} = 100$ mm, representing a more extreme, but possible, repository depth.

Set D: A single analysis, using the mid-range parameters without removing the tunnel lining in Phase (iii), simulating additional local support (see Scenario II in Figure 2.2(b)). An additional phase (v) has been added where local support is removed, to simulate using only temporary local support.

2.2 Results and discussion

This section presents the results of the simulations. The base case results are presented first and then the sensitivity analysis results are shown. The response of the Boom Clay, in terms of the extent of the Hardening Zone (HZ) and Plastic Zone (PZ), as well as the lining forces, are studied. The base case results are presented first and then the sensitivity analysis results are shown.

2.2.1 Base case results

A summary of the major impacts on the Boom Clay and the lining, for the base case, are presented in Table 2.3. A detailed discussion of the impact of the tunnel construction on the soil behaviour are presented first, followed by the impact on the tunnel lining.

Table 2.3: Summary of the main gallery response at different construction phases.

Phase	r_{PZ}^{h} * [m]	r_{PZ}^{v} [m]	r_{HZ}^{h} [m]	r_{HZ}^{v} [m]	$N_{1,max}$ $\left[\frac{kN}{m}\right]$	$N_{1,min}$ $\left[\frac{kN}{m}\right]$	$N_{2,max}$ $\left[\frac{kN}{m}\right]$	$N_{2,min}$ $\left[\frac{kN}{m}\right]$	$M_{l1,max}$ $\left[\frac{kN\ m}{m}\right]$	$M_{l1,min}$ $\left[\frac{kN\ m}{m}\right]$	$M_{22,max}$ $\left[\frac{kN\ m}{m}\right]$	$M_{22,min}$ $\left[\frac{kN\ m}{m}\right]$
(ii)	2.57	2.57	13.02	12.75	-586	-5089	-10820	-25040	107	-567	188	-532
(iii)	2.57	2.57	13.04	12.75	6785	-15520	1380	-55050	2143	-868	982	-2361
(iv)	2.57	2.57	13.04	12.75	561	-21180	-2995	-66900	2237	-1499	1048	-2512

* Plastic and Hardening radii are based on the cross section at y = 20 m.

r indicates the radius, superscripts h and v indicate horizontal and vertical directions, respectively, subscripts PZ and HZ indicate plastic and hardening zones, N_1 and N_2 are the longitudinal and hoop axial forces, M_{l1} and M_{22} are the longitudinal and hoop moments, and subscripts min and max indicate the minimum and maximum.

Impact on the Boom Clay

The behaviour of the Boom Clay in response to the construction phases is shown in Figure 2.3. The dark blue dots are the Gauss points in the mesh which are hardening, the red dots the Gauss points which are at failure. The light blue shading is an interpretation of the hardening zone. The concentration of the dark blue points in some locations is due to the higher level of discretisation of the mesh due to the same mesh being used in all phases. In Phase (ii) (shown in Figure 2.3(a,b)), the results are as expected, and similar to those of Arnold et al. (2015); i.e. a circular hardening and plastic failure zone, with the plastic failure zone limited in extent around the tunnel to a radius of approximately 2.6 m (where the external radius of the tunnel is 2.4 m). The hardening zone (where plastic deformation also occurs) is significantly larger, up to a radius of approximately 12.75 m. In Phase (iii), a highly localised extension to the plastic failure zone is seen in Figure 2.3(c), where the tunnel lining is removed locally. This has an almost imperceptible effect on the hardening zone.

Figure 2.4 shows the extent of the hardening and plastic zones after Phase (iv), where the disposal tunnel has been constructed. It can be seen, from the extent of the plastic and hardening zone at section A-A (Figure 2.4(b)), that 20 m away from the centre-line of the child tunnel, there is no perceptible impact on the plastic and hardening zones. Each tunnel can be seen to have its own distinct hardening zone (see Figure 2.4(a,d)), which is approximately circular (see e.g. Figure 2.4(b,f)), with the size largely controlled by only the tunnel radius, overcut and lining properties. The hardening zone around the child tunnel can be seen to decrease slightly along its length, moving away from the parent tunnel and becoming more circular (see e.g. Figure 2.4(e,f)). The transition between the two hardening zones and the two plastic zones has a small radius, less than 2 m, which implies that there is little extra damage to the Boom Clay.

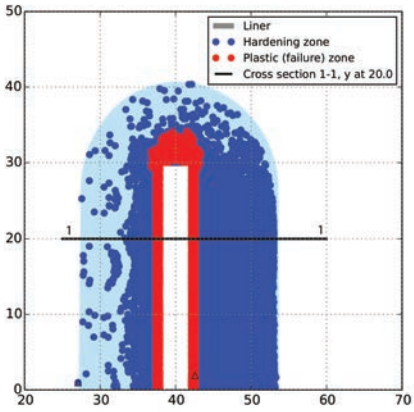

(a) x-y plane (500 m) Phase (ii)

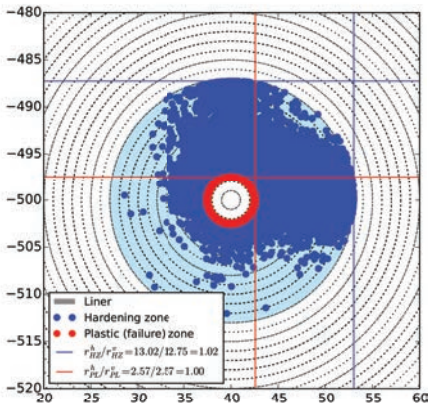

(b) Section 1-1 x-z plane Phase (ii)

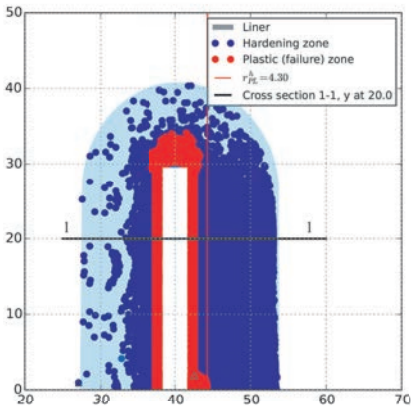

(c) x-y plane (500 m) Phase (iii)

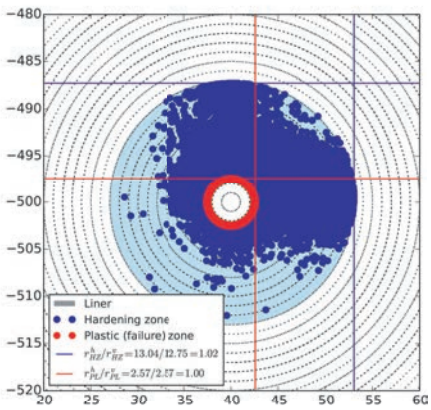

(d) Section 1-1 x-z plane Phase (iii)

Figure 2.3: Base case Boom Clay response (with $r_c = 2.4$ m, $d_{oc} = 75$ mm and $d = 500$ m): Gaussian integration points showing the extent of the *Plastic Zone* (PZ) and *Hardening Zone* (HZ): (a, b) Phase (ii) for the x-y and x-z planes, respectively, and (c,d) Phase (iii) for the x-y and x-z planes, respectively. The x and y coordinates are local to the mesh and the z coordinate is the depth.

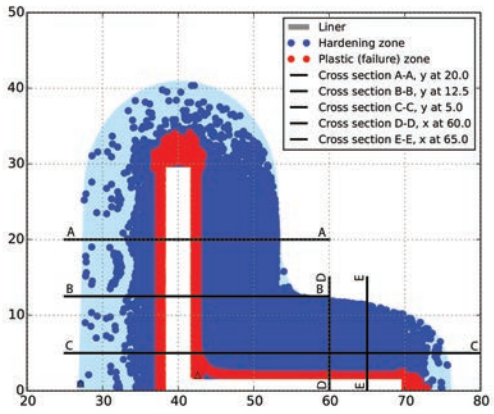

(a) x-y plane Phase (iv)

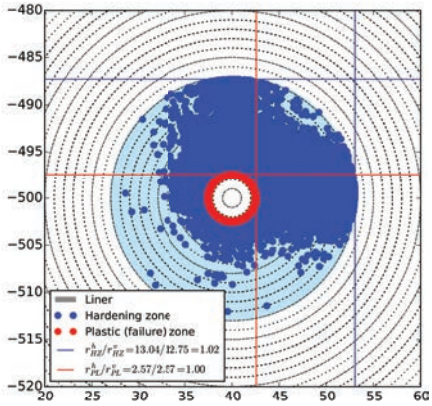

(b) Cross section A-A x-z plane Phase (iv)

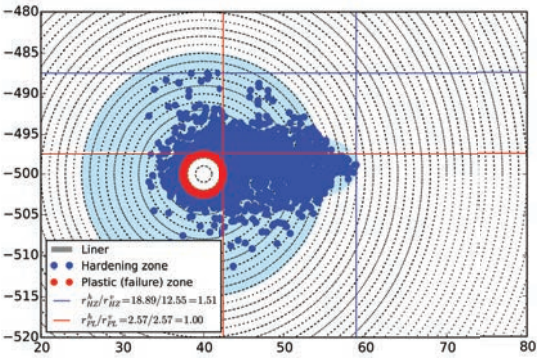

(c) Cross section B-B x-z plane Phase (iv)

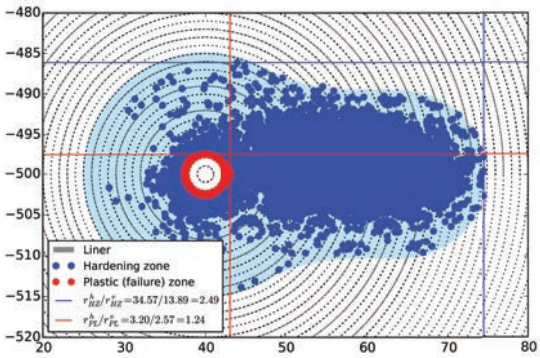

(d) Cross section C-C x-z plane Phase (iv)

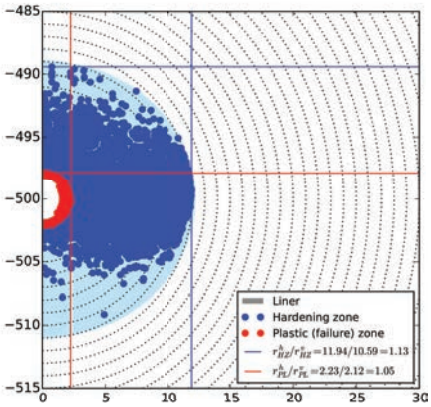

(e) Cross section D-D x-z plane Phase (iv)

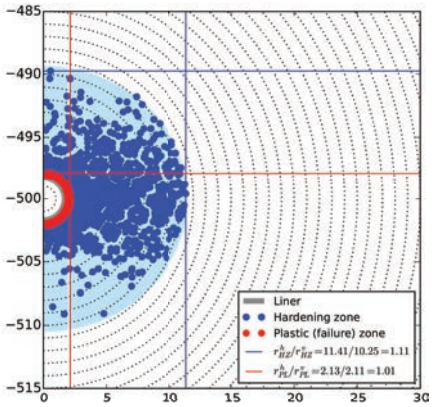

(f) Cross section E-E x-z plane Phase (iv)

Figure 2.4: Base case Boom Clay response (with main gallery $r_c = 2.4$ m, disposal tunnel $r_c = 1.6$ m, $d_{oc} = 75$ mm and $d = 500$ m): Gaussian integration points showing the extent of the *Plastic Zone* (PZ) and *Hardening Zone* (HZ): (a) Phase (iv) x-y (500 m) plane, (b,c,d) x-y plane $y = 5, 12.5$ and 20 m and (e,f) y-z plane $x = 60$ and 65 m.

Impact on the lining

Figure 2.5 presents the tunnel lining displacements for Phases (ii) until (iv). In Phase (ii), the tunnel displaces relatively uniformly, although the whole tunnel also ovalises slightly, as shown in the slight difference in the extent of the horizontal and vertical hardening zones in the Boom Clay. In Phase (iii), part of the tunnel lining is removed at the side of the tunnel, the lining displaces so that the top and the bottom of the tunnel move locally towards each other (ovalises) and the top and bottom of the tunnel opening also move towards each other (also ovalising). This is due to the loss of the arch effect of the tunnel. Similar deformed shapes to those shown in Spyridis and Bergmeister (2015) are found here. The crown and invert areas behave as flat arches/beams in the longitudinal directions, whereas, the same locations behave as cantilever beams in the hoop direction. In Phase (iv), the child tunnel is excavated and, as the soil presses against the new tunnel, displacement is seen. Less deformation is seen close to the parent tunnel, as the stresses here are already reduced (due to construction of the parent tunnel). In addition, the parent tunnel deforms further at the top and bottom (further ovalises), as hoop support from the Boom Clay is removed.

In Figure 2.6 the total normal stress on the lining can be seen. In Phase (ii), the normal stresses are almost uniform around the tunnel and along its length, as expected. There are limited effects at the end of the tunnel, which are a modelling artefact and should be ignored. In Phase (iii), due to the removal of the lining, additional load results locally around the tunnel opening, originating from the tunnel ovalisation (i.e. the tunnel pushes against the Boom Clay) and from the loss of support of the Boom Clay at the opening. In Phase (iv), as the Boom Clay at the location of the tunnel opening is excavated, the increase in stress immediately around the tunnel opening is reduced, but this in turn reduces the arch effect, which was previously supporting the Boom Clay around the tunnel and consequently increases the stress, to a distance of approximately 1 to 2 m around the tunnel opening. The stress on the child lining is similar in magnitude to that originally on the parent tunnel, and it is relatively uniform, except for near the parent tunnel where it is reduced for the same reasons outlined above. The stress level locally reaches approximately the same value as the insitu total stress (10 MPa), which is within the maximum lining compressive strength (approximately 12 MPa for a concrete compressive strength of 45 MPa and a lining thickness of 0.5 m - see Figure 4.4, Arnold et al. (2015)), although the stress differences will cause bending moments within the lining.

The differences in pressure on the lining cause the bending moments to increase considerably. These are presented in Figure 2.7, in terms of the longitudinal bending moments (bending along the direction of the tunnel) and hoop bending moments (bending around the circumference of the tunnel). The longitudinal and hoop bending moments increase very close to the opening in Phase (iii), significantly within around 1 child tunnel radius of the opening, and increase in extent to about 1.5 child tunnel radii in Phase (iv). Very localised high moments are observed at the horizontal edge of the child tunnel, due to the loss of Boom Clay arching around the main tunnel. These are within approximately 0.5 child tunnel radii in the longitudinal direction.

More details on the quantitative distribution of the bending moments in the main tunnel after Phase (iii) are presented in Figure 2.9. A polar coordinate system is adopted, where the angle 0° is the centre of the tunnel opening and 90° is the tunnel crown. Three sections are presented: 0 m, i.e. at the tunnel opening, 2.5 m away from the tunnel opening centre and 10 m away from the tunnel opening centre. The tunnel opening was located between approximately 315° and 45°.

It can be seen from Figure 2.9(a) that the longitudinal bending moment at the tunnel opening (y = 0 m) is significantly affected by the opening. The longitudinal bending moment is positive in the right half, whereas it is almost zero (but negative) in the left half. The maximum is reached at the tunnel opening. The longitudinal bending moment at the section 2.5 m away is only slightly affected by the tunnel opening. In Figure 2.9(b), in can be seen that the tunnel lining is affected around the entire circumference and has both positive and negative bending. The section at y = 2.5 m is also significantly affected, whereas the section at y = 10 m is slightly impacted. It is noted that the peak hoop moments are not seen in these figures, as these are are located at the edge of the opening and at 45° to the opening centreline (see Figure 2.7).

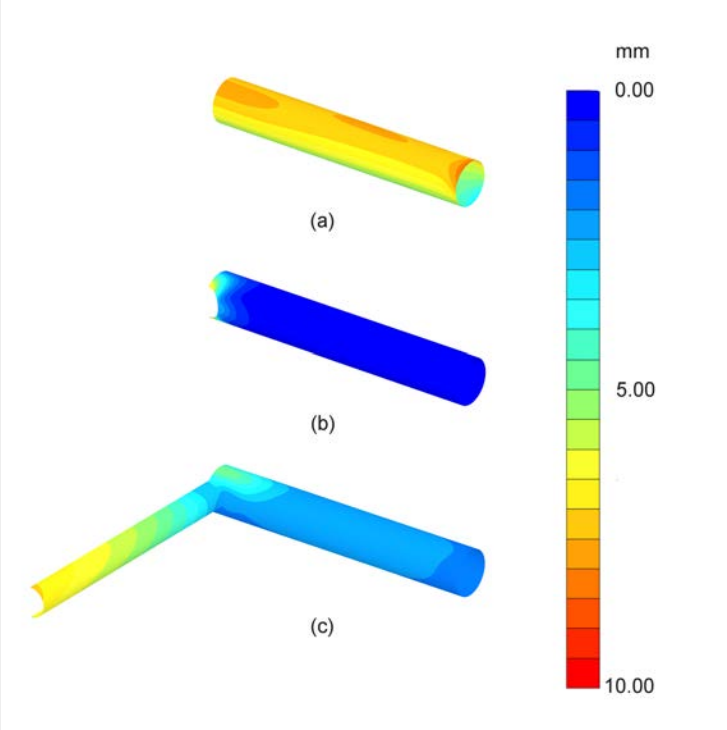

Figure 2.5: Displacements (magnitude) of the lining per phase: (a) Phase (ii), (b) Phase (iii) and (c) Phase (iv).

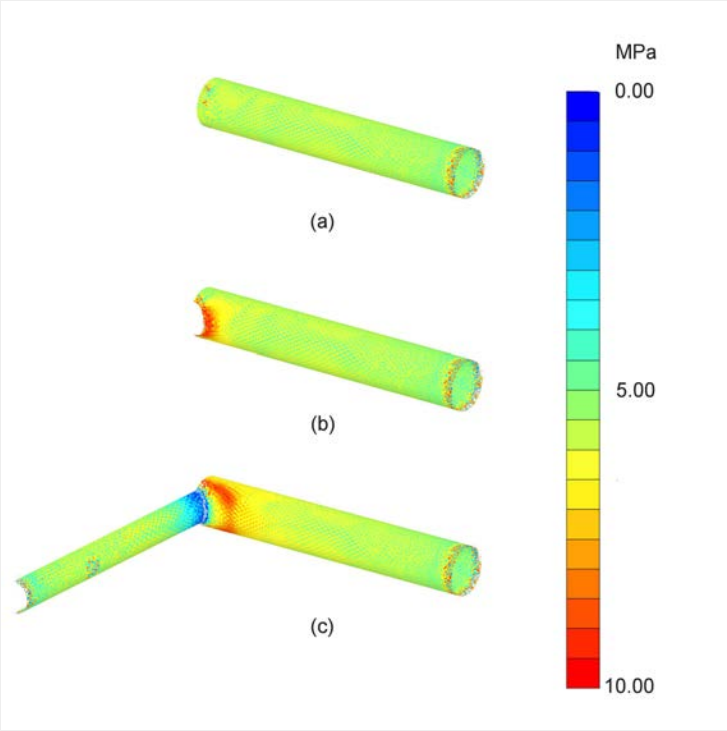

Figure 2.6: Normal (total) stress on the lining during: (a) Phase (ii), (b) Phase (iii) and (c) Phase (iv).

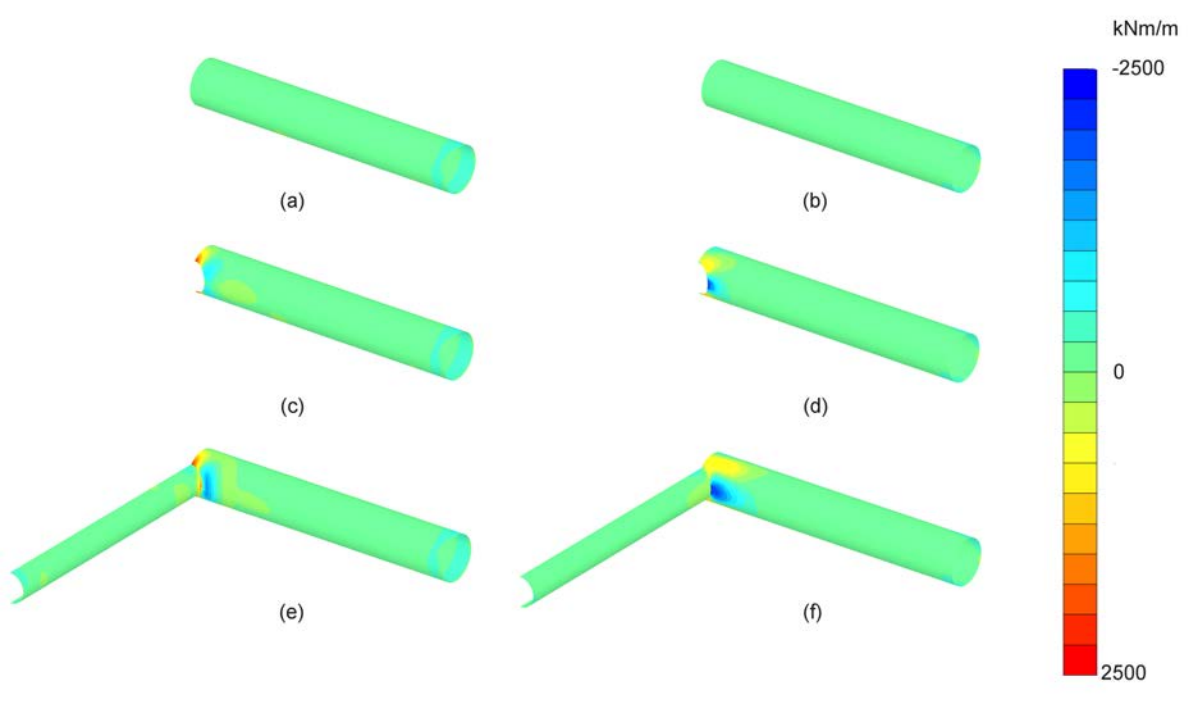

Figure 2.7: Moments acting on the lining per phase: (a) Phase (ii) longitudual, (b) Phase (ii) hoop, (c) Phase (iii) longitudual, (d) Phase (iii) hoop, (e) Phase (iv) longitudual, (f) Phase (iv) hoop.

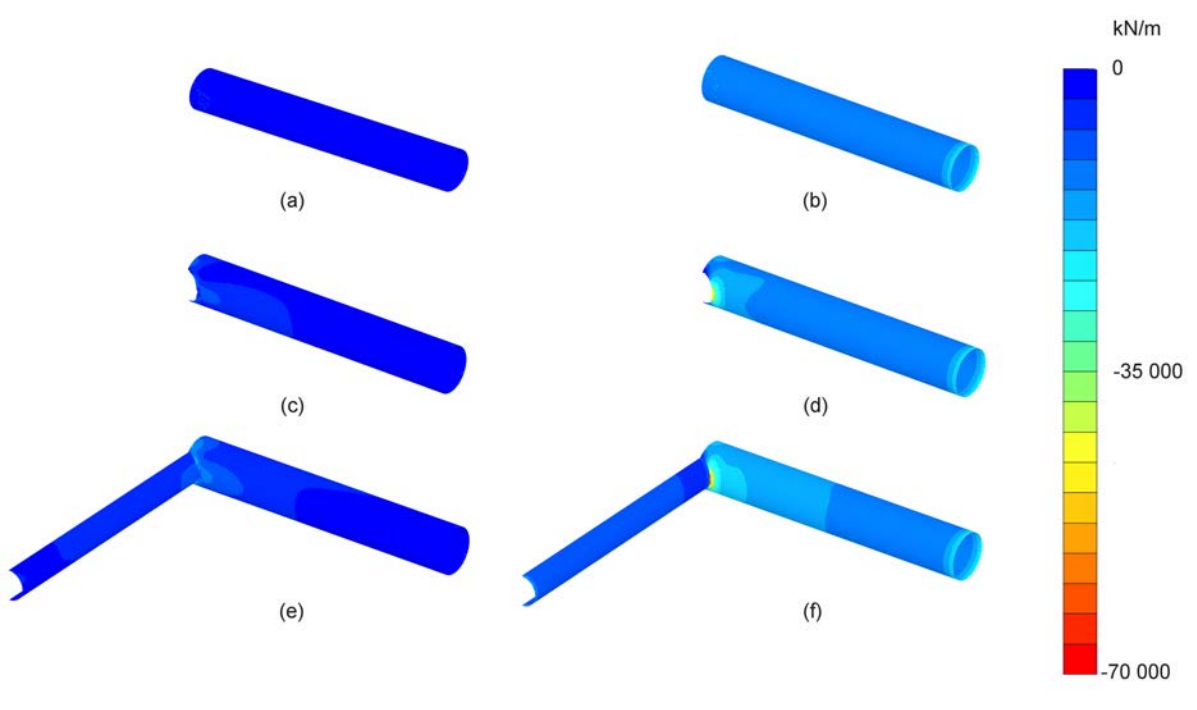

Figure 2.8: Forces acting on the lining per phase: (a) Phase (ii) longitudual, (b) Phase (ii) hoop, (c) Phase (iii) longitudual, (d) Phase (iii) hoop, (e) Phase (iv) longitudual, (f) Phase (iv) hoop. Sign convention is compression negative.

The forces in the lining are presented in Figure 2.8, where the sign convention is compression negative, with the longitudinal forces showing only minor increases close to the child tunnel. The hoop forces are seen to increase, strongly adjacent to the child tunnel and moderately until around 5 child tunnel radii from the tunnel. There are increased forces in the child tunnel lining close to the tunnel opening, although these are lower than in the main tunnel and are therefore less obvious in the figure. Tensile longitudinal axial forces are found at the crown and invert areas of the tunnel opening (Phases (iii) and (iv)), although they are limited in extent and magnitude. However, larger tension areas lie further away from the opening in a diagonal direction of approximately 45°. The maximum compressive longitudinal axial forces (called minimum longitudinal forces in the tables presented in Section 2.2.2) are found at a diagonal direction of approximately 45°, very close to the opening, with further compressive zones of a greater extent at 0 and 90°. The largest tensile hoop axial forces are found at the crown and invert areas, although again the extent and magnitude are limited. The maximum compressive hoop axial forces are found in the springline area (the line midway between the crown and the invert). It can be seen that the longitudinal axial forces are mainly negative, which means that the tunnel lining over the entire section is compressed except at the crown and invert areas. Reinforcement such as thickening at the sides, or steel reinforcement of the opening, is probably necessary.

The quantitative distribution of the axial forces in the longitudinal and hoop directions is shown in Figure 2.9(c,d), again using polar coordinates around the main tunnel. It can be seen that the axial forces were negative in all the sections, which means that the tunnel lining was compressed. The hoop forces follow a similar trend to the longitudinal moments and vice versa. Limited additional forces are seen, with the hoop axial forces reducing close to the opening. This is due to the major increases in axial hoop stress being at the springline and therefore not represented in this figure.

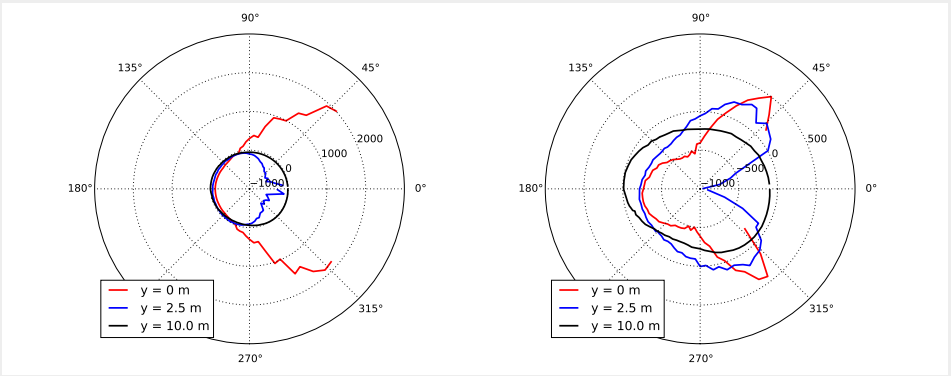

(a) Longitudinal moments (b) Hoop moments

(c) Longitudinal axial forces (d) Hoop axial forces

Figure 2.9: Distributions of the moments (kNm/m) and forces (kN/m) in Phase (iii) at the different tunnel sections: (a) Longitudinal moments; (b) Hoop moments; (c) Longitudinal axial forces; (d) Hoop axial forces. Note that the radial axis values are different on each sub-figure.

Discussion and summary

The results from a parent and child tunnel crossing simulation have been presented in the context of the construction of the proposed Dutch radioactive waste repository. It was seen that the change in the plastic behaviour, and therefore the excavated damaged zone in the clay, does not significantly increase beyond that of a single tunnel excavation, and is therefore unlikely to significantly affect the performance of the repository.

However, due to the removal of the tunnel lining for the child tunnel and the consequential excavation of the child tunnel, a significant redistribution of stress takes place, leading to localised stress differences in the lining and large increases in the bending moments. These should be taken into account in the detailed design and it is likely that substantial local reinforcement will be needed. This means an increase in the amount of steel in the repository, which can corrode in time, potentially leading to hydrogen gas generation and a possible impact on long term retrievability.

2.2.2 Sensitivity analysis results

The entire register of results for three phases of the main and disposal tunnels can be found for Phase (ii) in Table 2.4, for Phase (iii) in Table 2.5 and for Phase (iv) in Tables 2.6 and 2.7 for the parent and the child tunnels, respectively. Note that the horizontal and vertical radii of the hardening zone (HZ) and plastic failure zone (PZ) for the parent tunnel are evaluated at the cross section at y= 20 m and for the disposal (child) tunnel are evaluated at the cross section at x= 65 m.

2.2.2.1 Impact on the Boom Clay

The response of the Boom Clay in terms of the extent of the HZ and PZ at different excavation phases due to variation of model parameters, state variable and boundary conditions are studied in this section.

Phase (ii) Main gallery excavation phase

Figure 2.10 compares the impact of the four key parameters on the hardening and plastic zones for Phase (ii) - similar to the comparison shown in Arnold et al. (2015). The blue lines represent Set A, the red, Set B and the green, Set C. An increase in the strength parameters, i.e. cohesion and friction angle, c' and ϕ', respectively, reduces the plastic and hardening radii (see Figure 2.10 (a-b)). The extent of the hardening radii are significantly larger than the extent of the perfectly plastic radii, with the latter defining stress states located on the failure envelop.

For $K_0 = 1$, the response is isotropic and $r^h \approx r^v$ (see Table 2.4). However, it is possible that the in situ stress is anisotropic, i.e. corresponding to the earth pressure at rest being $K_0 < 1$ (Arnold et al., 2015). Figure 2.10 shows the hardening and plastic radial in the horizontal direction with different K_0 values. With increasing degree of in situ stress anisotropy (reducing K_0), the extent of the hardening in the horizontal direction becomes significantly larger than in the vertical direction (see Table 2.4 and Figure 2.11 (b-d)). The hardening zone extending in diagonal direction from the tunnel in Figure 2.11 (d) for a low earth pressure coefficient at rest of $K_0 = 0.8$ is due to the shear hardening surface being reached earlier due to the shear stresses induced by the in situ stress anisotropy. Considering the effect of different boundary conditions, i.e. of increasing the overcut d_{oc} to 100 mm and the depth d to 700 m, changing the overcut has the greater impact on the extent of the hardening and plastic radii (Figure 2.10). However, the extent of the plastic zone is less sensitive to a value of the variation in both d_{oc} and d (note the minimum radius is the outer radius of the tunnel, i.e. 2.4ṁ; zero in the figure indicates no plastic points).

Table 2.4: Main gallery response due to variation of model parameters in Phase (ii).

Set	Var. X	Unit	Val.	r_{PZ}^{h} * [m]	r_{PZ}^{v} [m]	r_{HZ}^{h} [m]	r_{HZ}^{v} [m]	$N_{1,max}$ $\left[\frac{\text{kN}}{\text{m}}\right]$	$N_{1,min}$ $\left[\frac{\text{kN}}{\text{m}}\right]$	$N_{2,max}$ $\left[\frac{\text{kN}}{\text{m}}\right]$	$N_{2,min}$ $\left[\frac{\text{kN}}{\text{m}}\right]$	$M_{l1,max}$ $\left[\frac{\text{kN m}}{\text{m}}\right]$	$M_{l1,min}$ $\left[\frac{\text{kN m}}{\text{m}}\right]$	$M_{22,max}$ $\left[\frac{\text{kN m}}{\text{m}}\right]$	$M_{22,min}$ $\left[\frac{\text{kN m}}{\text{m}}\right]$
A	c'	[MPa]	0.30	3.11	3.14	15.36	14.83	-124.1	-4571	-10870	-26240	90.79	-466.3	94.84	-525.7
			0.50	2.57	2.57	13.02	12.75	-585.8	-5089	-10820	-25040	107	-566.7	187.7	-531.8
			0.70	2.57	2.57	11.76	11.61	-992.3	-5745	-10770	-23410	109.2	-620.0	250.2	-530
	ϕ'	[°]	7.50	2.67	2.67	13.50	13.07	1252	-3384	-13240	-29860	76.01	-465.2	-73.5	-499.5
			12.50	2.57	2.57	13.02	12.75	-585.8	-5089	-10820	-25040	107	-566.7	187.7	-531.8
			17.50	2.57	2.57	11.98	11.80	-1514	-6788	-8071	-18920	108.9	-612.1	372.9	-524
	E_{50}^{ref}	[MPa]	80.00	0**	0**	12.92	12.61	-501.4	-4946	-11430	-26550	-100.2	-570.9	126.9	-531.2
			120.00	2.57	2.57	13.02	12.75	-585.8	-5089	-10820	-25040	107	-566.7	187.7	-531.8
			160.00	3.28	3.30	12.65	12.43	-657.7	-5253	-10250	-23680	111	559.5	235.3	-523.7
	K_0	[–]	0.8	0**	0**	19.41	14.39	-375.2	-5272	-10670	-24770	93.21	-567	620.6	-862
			0.9	2.57	2.57	15.53	10.14	-458.4	-5011	-10640	-24840	100.4	-569.6	437.7	-655.4
			1.0	2.57	2.57	13.02	12.75	-585.8	-5089	-10820	-25040	107	-566.7	187.7	-531.8
B	c'	[MPa]	0.30	3.58	3.63	17.69	16.91	-62.04	-4884	-10080	-25220	114.8	-483.5	225.5	-539.7
			0.50	2.88	2.91	14.99	14.58	-571.4	-5819	-10010	-23620	130	-574.5	335.8	-549.2
			0.70	2.57	2.57	13.56	13.27	-986.1	-6598	-9415	-21480	133.3	-625.3	412	-548.9
	ϕ'	[°]	7.50	3.30	3.30	17.51	16.72	492.8	-4237	-12070	-29580	77.66	-487.6	-26.58	-457.4
			12.50	2.88	2.91	14.99	14.58	-571.4	-5819	-10010	-23620	130	-574.5	335.8	-549.2
			17.50	2.57	2.57	13.71	13.42	-1459	-7831	-6609	-17310	136.7	-610	517	-559.3
	E_{50}^{ref}	[MPa]	80.00	2.57	2.57	14.89	14.40	-525.2	-5569	-10650	-25150	122.7	-582.4	271.1	-554.4
			120.00	2.88	2.91	14.99	14.58	-571.4	-5819	-10010	-23620	130	-574.5	335.8	-549.2
			160.00	3.78	3.76	14.53	14.17	-485.8	-5958	-9235	-22320	134.6	-573.6	404.6	-545.9
	K_0	[–]	0.8	2.96	2.90	21.74	16.32	-373.2	-5338	-9935	-23480	117.5	-573.7	745.4	-859.1
			0.9	2.90	2.93	17.79	11.58	-479.8	-5612	-9868	-23380	123.9	-574.2	566.3	-651.6
			1.0	2.88	2.91	14.99	14.58	-571.4	-5819	-10010	-23620	130	-574.5	335.8	-549.2
C	c'	[MPa]	0.30	3.05	3.06	14.80	14.05	462	-5511	-16000	-39100	91.59	-496	31.22	-772
			0.50	2.57	2.57	12.42	11.95	209.2	-6214	-16290	-38240	90.69	-645.9	66.45	-898
			0.70	0**	0**	10.97	10.69	-232.1	-6589	-16540	-36810	93.2	-704.8	54.19	-924.8
	ϕ'	[°]	7.50	-***	-***	-***	-***	-***	-***	-***	-***	-***	-***	-***	-***
			12.50	2.57	2.57	12.42	11.95	209.2	-6214	-16290	-38240	90.69	-645.9	66.45	-898
			17.50	2.57	2.57	11.41	11.09	-1237	-7259	-13760	-28990	90.72	-694.5	160.9	-869.5
	E_{50}^{ref}	[MPa]	80.00	2.57	2.57	11.41	11.09	302.6	-6067	-17010	-39900	94.07	-620.8	51.76	-860.6
			120.00	2.57	2.57	12.42	11.95	209.2	-6214	-16290	-38240	90.69	-645.9	66.45	-898
			160.00	3.21	3.21	12.40	12.01	95.1	-6239	-15660	-36680	98.65	-658.9	56.69	-905.9
	K_0	[–]	0.8	2.57	2.57	20.16	15.35	301.3	-6646	-16080	-37900	112.2	-658	616.9	-1381
			0.9	2.57	2.57	14.92	9.70	223.3	-6301	-16030	-37940	102.6	-662.4	369.8	-1160
			1.0	2.57	2.57	12.42	11.95	209.2	-6214	-16290	-38240	90.69	-645.9	66.45	-898
D	[–]	[–]	[–]	2.57	2.57	13.02	12.75	-585.8	-5089	-10820	-25040	107	-566.7	187.7	-531.8

Set A: Variation of four variables with $d_{oc} = 75$mm and $d = 500$m. Set B: Variation of four variables with $d_{oc} = 100$mm and $d = 500$m. Set C: Variation of four variables with $d_{oc} = 75$mm and $d = 700$m. Set D: Reference model with support at the liner opening for gallery with $d_{oc} = 75$mm and $d = 500$m.

* Plastic and Hardening radius are based on the cross section at y = 20 m. ** Failure surface not reached. *** Calculation failure due to soilbody collapse in Plaxis.

Table 2.5: Main gallery response due to variation of model parameters in Phase (iii).

Set	Var. X	Unit	Val.	r_{PZ}^{h} * [m]	r_{PZ}^{v} [m]	r_{HZ}^{h} [m]	r_{HZ}^{v} [m]	$N_{1,max}$ $\left[\frac{\text{kN}}{\text{m}}\right]$	$N_{1,min}$ $\left[\frac{\text{kN}}{\text{m}}\right]$	$N_{2,max}$ $\left[\frac{\text{kN}}{\text{m}}\right]$	$N_{2,min}$ $\left[\frac{\text{kN}}{\text{m}}\right]$	$M_{l1,max}$ $\left[\frac{\text{kN m}}{\text{m}}\right]$	$M_{l1,min}$ $\left[\frac{\text{kN m}}{\text{m}}\right]$	$M_{22,max}$ $\left[\frac{\text{kN m}}{\text{m}}\right]$	$M_{22,min}$ $\left[\frac{\text{kN m}}{\text{m}}\right]$
A	c'	[MPa]	0.30	3.11	3.14	15.42	14.83	7447	-14870	1442	-51750	2128	-947	1090	-2678
			0.50	2.57	2.57	13.04	12.75	6785	-15520	1380	-55050	2143	-868	982.3	-2361
			0.70	2.57	2.57	11.77	11.61	6638	-15600	1362	-55960	2110	-812.6	921.3	-2177
	ϕ'	[°]	7.50	2.68	2.67	13.64	13.07	27630	-16130	3442	-58240	2905	-1439	1707	-4618
			12.50	2.57	2.57	13.04	12.75	6785	-15520	1380	-55050	2143	-868	982.3	-2361
			17.50	2.57	2.57	11.98	11.80	2880	-13060	866.1	-47420	1592	-625.7	630.9	-1366
	E_{50}^{ref}	[MPa]	80.00	0**	0**	12.94	12.61	9772	-16160	1696	-57170	2348	-979.5	1121	-2754
			120.00	2.57	2.57	13.04	12.75	6785	-15520	1380	-55050	2143	-868	982.3	-2361
			160.00	3.28	3.30	12.66	12.43	4854	-14890	1162	-53010	1991	-789.5	888.9	-2073
	K_0	[–]	0.8	0**	0**	19.41	14.39	6711	-14940	1352	-52230	2026	-858.5	972.5	-2087
			0.9	2.57	2.57	15.56	10.14	6791	-15100	1369	-53260	2055	-845.4	959.1	-2140
			1.0	2.57	2.57	13.04	12.75	6785	-15520	1380	-55050	2143	-868	982.3	-2361
B	c'	[MPa]	0.30	3.58	3.63	17.70	16.91	5521	-14140	1214	-49170	1947	-841.6	969.5	-2324
			0.50	2.88	2.91	15.00	14.58	4880	-14620	1144	-51910	1967	-770.5	885.5	-2014
			0.70	2.57	2.57	13.56	13.27	4482	-14550	1059	-52070	1928	-723.4	823.2	-1845
	ϕ'	[°]	7.50	3.30	3.30	17.62	16.72	17730	-16050	2490	-55690	2761	-1337	1638	-4275
			12.50	2.88	2.91	15.00	14.58	4880	-14620	1144	-51910	1967	-770.5	885.5	-2014
			17.50	2.57	2.57	13.71	13.42	2350	-11760	632.3	-42200	1415	-609.7	532.7	-1126
	E_{50}^{ref}	[MPa]	80.00	2.57	2.57	14.92	14.40	7437	-15360	1426	-54330	2164	-870.8	1002	-2376
			120.00	2.88	2.91	15.00	14.58	4880	-14620	1144	-51910	1967	-770.5	885.5	-2014
			160.00	3.78	3.76	14.54	14.17	3286	-13870	956.9	-49310	1809	-695.9	796.2	-1764
	K_0	[–]	0.8	2.96	2.90	21.83	16.32	4767	-14210	1102	-49640	1877	-764.3	887.9	-1777
			0.9	2.90	2.93	17.83	11.58	4641	-14310	1107	-50440	1895	-750.5	870.2	-1829
			1.0	2.88	2.91	15.00	14.58	4880	-14620	1144	-51910	1967	-770.5	885.5	-2014
C	c'	[MPa]	0.30	3.05	3.06	14.85	14.05	16580	-20880	2713	-72520	3253	-1549	1792	-4681
			0.50	2.57	2.57	12.43	11.95	14530	-22320	2503	-78190	3250	-1434	1656	-4197
			0.70	0**	0**	10.99	10.69	14690	-23160	2520	-82160	3290	-1376	1548	-3935
	ϕ'	[°]	7.50	-***	-***	-***	-***	-***	-***	-***	-***	-***	-***	-***	-***
			12.50	2.57	2.57	12.43	11.95	14530	-22320	2503	-78190	3250	-1434	1656	-4197
			17.50	2.57	2.57	11.41	11.09	7611	-19530	1620	-71140	2415	-930.2	1010	-2373
	E_{50}^{ref}	[MPa]	80.00	2.57	2.57	12.31	11.77	19890	-22810	3045	-80220	3520	-1585	1847	-4767
			120.00	2.57	2.57	12.43	11.95	14530	-22320	2503	-78190	3250	-1434	1656	-4197
			160.00	3.21	3.21	12.42	12.01	11250	-21750	2164	-76210	3045	-1323	1510	-3800
	K_0	[–]	0.8	2.57	2.57	20.25	15.62	15950	-21110	2629	-73450	3116	-1455	1657	-3969
			0.9	2.57	2.57	14.92	9.70	15070	-21550	2537	-75300	3124	-1411	1619	-3916
			1.0	2.57	2.57	12.43	11.95	14530	-22320	2503	-78190	3250	-1434	1656	-4197
D	[–]	[–]	[-]	2.57	2.57	13.02	12.75	-585.8	-5089	-10820	-25040	107	-566.7	187.7	-531.8

Set A: Variation of four variables with $d_{oc} = 75$mm and $d = 500$m. Set B: Variation of four variables with $d_{oc} = 100$mm and $d = 500$m. Set C: Variation of four variables with $d_{oc} = 75$mm and $d = 700$m. Set D: Reference model with support at the liner opening for gallery with $d_{oc} = 75$mm and $d = 500$m.

* Plastic and Hardening radius are based on the cross section at y = 20 m. ** Failure surface not reached. *** Calculation failure due to soilbody collapse in Plaxis.

Table 2.6: Main gallery response due to variation of model parameters in Phase (iv).

Set	Var. X	Unit	Val.	r_{PZ}^{h} * [m]	r_{PZ}^{v} [m]	r_{HZ}^{h} [m]	r_{HZ}^{v} [m]	$N_{1,max}$ $\left[\frac{\text{kN}}{\text{m}}\right]$	$N_{1,min}$ $\left[\frac{\text{kN}}{\text{m}}\right]$	$N_{2,max}$ $\left[\frac{\text{kN}}{\text{m}}\right]$	$N_{2,min}$ $\left[\frac{\text{kN}}{\text{m}}\right]$	$M_{l1,max}$ $\left[\frac{\text{kN m}}{\text{m}}\right]$	$M_{l1,min}$ $\left[\frac{\text{kN m}}{\text{m}}\right]$	$M_{22,max}$ $\left[\frac{\text{kN m}}{\text{m}}\right]$	$M_{22,min}$ $\left[\frac{\text{kN m}}{\text{m}}\right]$
A	c'	[MPa]	0.30	3.11	3.14	16.30	14.83	318.5	-20370	-3909	-65060	2366	-1410	1298	-2669
			0.50	2.57	2.57	13.04	12.75	561.4	-21180	-2995	-66900	2237	-1499	1048	-2512
			0.70	2.57	2.57	11.77	11.61	670.5	-21280	-2403	-66860	2096	-1503	1081	-2435
	ϕ'	[°]	7.50	2.70	2.67	14.45	13.07	19060	-21200	-1027	-69110	3099	-1471	1559	-4476
			12.50	2.57	2.57	13.04	12.75	561.4	-21180	-2995	-66900	2237	-1499	1048	-2512
			17.50	2.57	2.57	12.22	11.80	-691.8	-20050	-3862	-59130	2082	-1481	899.4	-1699
	E_{50}^{ref}	[MPa]	80.00	0**	0**	13.75	12.61	3206	-22360	-92.50	-74440	2641	-1829	1632	-3264
			120.00	2.57	2.57	13.04	12.75	561.4	-21180	-2995	-66900	2237	-1499	1048	-2512
			160.00	3.28	3.30	12.93	12.43	288	-20790	-3553	-64510	2121	-1515	1011	-2243
	K_0	[–]	0.8	2.64	2.57	22.59	16.32	737.3	-19120	-3141	-63680	2193	-1380	1069	-2164
			0.9	2.57	2.57	16.32	10.14	646.9	-19980	-3185	-64510	2172	-1420	1068	-2229
			1.0	2.57	2.57	13.04	12.75	561.4	-21180	-2995	-66900	2237	-1499	1048	-2512
B	c'	[MPa]	0.30	3.58	3.63	19.71	16.91	-4.939	-20340	-5002	-63500	2558	-1420	1395	-2288
			0.50	2.88	2.91	15.78	14.58	-296.4	-21420	-4308	-64850	2415	-1539	1147	-2144
			0.70	2.57	2.57	13.98	13.27	-385.6	-21860	-4027	-64450	2326	-1150	1019	-2071
	ϕ'	[°]	7.50	3.31	3.30	19.56	16.72	8655	-21610	-3517	-68700	3025	-1454	1635	-4044
			12.50	2.88	2.91	15.78	14.58	-296.4	-21420	-4308	-64850	2415	-1539	1147	-2144
			17.50	2.57	2.57	13.71	13.42	-1325	-20800	-5386	-54850	-2405	-1471	981.3	-1502
	E_{50}^{ref}	[MPa]	80.00	2.57	2.57	15.67	14.40	191.1	-21450	-3309	-67320	2305	-1499	1152	-2493
			120.00	2.88	2.91	15.78	14.58	-296.4	-21420	-4308	-64850	2415	-1539	1147	-2144
			160.00	3.79	3.76	15.08	14.17	-419	-21450	-4722	-62180	2404	-1524	1107	-1919
	K_0	[–]	0.8	2.97	2.90	28.34	20.18	-83.94	-19180	-4325	-62390	2273	-1414	1166	-1836
			0.9	2.90	2.93	19.38	11.58	-204	-20190	-4437	62970	2338	-1461	1168	-1904
			1.0	2.88	2.91	15.78	14.58	-296.4	-21420	-4308	-64850	2415	-1539	1147	-2144
C	c'	[MPa]	0.30	3.05	3.06	15.56	14.05	7178	-27230	-4641	-89280	3678	-1899	1933	-4447
			0.50	2.57	2.57	12.74	11.95	4893	-28680	-3201	-93500	3536	-1975	1585	-4186
			0.70	2.55	2.53	11.23	10.69	4529	-29730	-2454	-96640	3481	-2035	1423	-4046
	ϕ'	[°]	7.50	-***	-***	-***	-***	-***	-***	-***	-***	-***	-***	-***	-***
			12.50	2.57	2.57	12.74	11.95	4893	-28680	-3201	-93500	3536	-1975	1585	-4186
			17.50	2.57	2.57	11.61	11.09	810.6	-27130	-4258	-85820	2525	-2002	1227	-2654
	E_{50}^{ref}	[MPa]	80.00	2.57	2.57	12.63	11.77	11280	-28810	-2217	-95360	3850	-1960	1629	-4713
			120.00	2.57	2.57	12.74	11.95	4893	-28680	-3201	-93500	3536	-1975	1585	-4186
			160.00	3.21	3.21	12.68	12.01	1895	-28340	-4059	-91310	3294	-1991	1564	-3794
	K_0	[–]	0.8	2.57	2.57	23.25	17.76	8568	-25970	-3457	-88310	3478	-1831	1652	-3845
			0.9	2.57	2.57	15.62	9.70	6702	-26990	-3138	-89800	3421	-1864	1568	-3858
			1.0	2.57	2.57	12.74	11.95	4893	-28680	-3201	-93500	3536	-1975	1585	-4186
D	[–]	[–]	[-]	2.57	2.57	13.02	12.75	-528.8	-10890	-11770	-24930	1599	-562.9	1121	-1004

Set A: Variation of four variables with $d_{oc} = 75$mm and $d = 500$m. Set B: Variation of four variables with $d_{oc} = 100$mm and $d = 500$m. Set C: Variation of four variables with $d_{oc} = 75$mm and $d = 700$m. Set D: Reference model with support at the liner opening for gallery with $d_{oc} = 75$mm and $d = 500$m.

* Plastic and Hardening radius are based on the cross section at y = 20 m. ** Failure surface not reached. *** Calculation failure due to soilbody collapse in Plaxis.

Table 2.7: Disposal (child) tunnel response due to variation of model parameters in Phase (iv).

Set	Var. X	Unit	Val.	r_{PZ}^{h} * [m]	r_{PZ}^{v} [m]	r_{HZ}^{h} [m]	r_{HZ}^{v} [m]	$N_{1,max}$ [kN/m]	$N_{1,min}$ [kN/m]	$N_{2,max}$ [kN/m]	$N_{2,min}$ [kN/m]	$M_{l1,max}$ [kN m/m]	$M_{l1,min}$ [kN m/m]	$M_{22,max}$ [kN m/m]	$M_{22,min}$ [kN m/m]
A	c'	[MPa]	0.30	2.65	2.63	13.64	11.65	-597.9	-10110	-4107	-17970	1861	-412.8	304.2	-323.9
			0.50	2.13	2.11	11.41	10.25	-1130	-10230	-3757	-17560	1680	-439.3	326.6	-324.7
			0.70	1.86	1.86	10.20	8.60	-1939	-10110	-3364	-15870	1544	-544.4	335.7	-377
	ϕ'	[°]	7.50	2.40	2.38	13.21	11.65	-2007	-11380	-3227	-15990	2180	-421.9	401.3	-322.2
			12.50	2.13	2.11	11.41	10.25	-1130	-10230	-3757	-17560	1680	-439.3	326.6	-324.7
			17.50	1.98	1.92	10.42	9.67	-2309	-11370	-1467	-13560	1762	-675.1	426.1	-449.6
	E_{50}^{ref}	[MPa]	80.00	3.03	3.24	14.80	13.66	-685.9	-12300	-3649	-18180	1721	-582.7	172.9	-422.9
			120.00	2.13	2.11	11.41	10.25	-1130	-10230	-3757	-17560	1680	-439.3	326.6	-324.7
			160.00	2.81	2.68	10.95	10.25	-1832	-10640	-3232	-15380	1725	490.7	367.4	-378.8
	K_0	[–]	0.8	2.17	2.13	17.74	15.05	-910.6	-9733	-3998	-17370	1570	-444.9	250.8	-447.7
			0.9	2.13	2.16	13.18	8.6	-1734	-9929	-3795	-16060	1632	-428.8	304	-352.8
			1.0	2.13	2.11	11.41	10.25	-1130	-10230	-3757	-17560	1680	-439.3	326.6	-324.7
B	c'	[MPa]	0.30	3.06	3.24	15.91	14.69	-2007	-11380	-3227	-15990	2180	-421.9	401.3	-322.2
			0.50	2.45	2.46	13.21	11.65	-1301	-11670	-2626	-16880	2025	-521.4	446.9	-416.4
			0.70	2.13	2.10	11.90	11.05	-2086	-11680	-2199	-14840	1952	-645.2	473.6	-479.6
	ϕ'	[°]	7.50	2.81	2.68	15.72	13.66	563.9	-8317	-5564	-20420	1877	-408	387.3	-403.5
			12.50	2.45	2.46	13.21	11.65	-1301	-11670	-2626	-16880	2025	-521.4	446.9	-416.4
			17.50	2.17	2.26	11.99	11.05	-2508	-12490	-120.1	-12860	2128	-762.6	570.3	-567.3
	E_{50}^{ref}	[MPa]	80.00	1.86	1.86	13.21	11.65	-1188	-10760	-3414	-17520	1872	-453	367.9	-339.2
			120.00	2.45	2.46	13.21	11.65	-1301	-11670	-2626	-16880	2025	-521.4	446.9	-416.4
			160.00	3.22	3.24	12.72	11.65	-2010	-11850	-2139	-14620	2046	-576.7	473	-458.8
	K_0	[–]	0.8	2.50	2.49	23.96	19.66	-1045	-11150	-3096	-17120	1905	-437.7	349.2	-405.2
			0.9	2.46	2.52	15.39	9.67	-2000	-11360	-2790	-15310	1969	-453.2	410.8	-368.1
			1.0	2.45	2.46	13.21	11.65	-1301	-11670	-2626	-16880	2025	-521.4	446.9	-416.4
C	c'	[MPa]	0.30	2.57	2.60	12.92	10.51	346.5	-11870	-7074	28010	2221	-490.6	389.5	-585.4
			0.50	2.09	2.13	10.64	9.55	-1148	-12460	-7010	-27680	1993	-594.5	363.1	-579.4
			0.70	1.86	1.86	9.60	8.79	-1952	-12850	-6954	-26340	1872	-649.8	373.5	-559.2
	ϕ'	[°]	7.50	-***	-***	-***	-***	-***	-***	-***	-***	-***	-***	-***	-***
			12.50	2.09	2.13	10.64	9.55	-1148	-12460	-7010	-27680	1993	-594.5	363.1	-579.4
			17.50	1.92	1.86	9.80	8.79	-3050	-15260	-3945	-21240	2112	-688.9	505.3	-464.8
	E_{50}^{ref}	[MPa]	80.00	1.86	1.86	10.64	9.55	-2806	-11240	-7768	-25830	1845	-659.3	300.7	-501.4
			120.00	2.09	2.13	10.64	9.55	-1148	-12460	-7010	-27680	1993	-594.5	363.1	-579.4
			160.00	2.72	2.64	10.64	9.55	-1459	-13350	-6382	-26220	2128	-586.5	422.9	-566.2
	K_0	[–]	0.8	2.14	2.13	18.11	16.66	-578.7	-11150	-6790	-27570	1859	-569	286.3	-584.5
			0.9	2.09	2.13	12.61	7.91	-903	-11620	-7052	-27470	1867	-580.4	320.5	-463.3
			1.0	2.09	2.13	10.64	9.55	-1148	-12460	-7010	-27680	1993	-594.5	363.1	-579.4
D	[–]	[–]	[-]	2.13	2.11	11.41	10.25	-1115	-13580	-1650	-17650	94.9	-1057	65.8	-467.1

Set A: Variation of four variables with $d_{oc} = 75$mm and $d = 500$m. Set B: Variation of four variables with $d_{oc} = 100$mm and $d = 500$m. Set C: Variation of four variables with $d_{oc} = 75$mm and $d = 700$m. Set D: Reference model with support at the liner opening for gallery with $d_{oc} = 75$mm and $d = 500$m.

* Plastic and Hardening radius are based on the cross section at x = 65 m. ** Failure surface not reached. *** Calculation failure due to soilbody collapse in Plaxis.

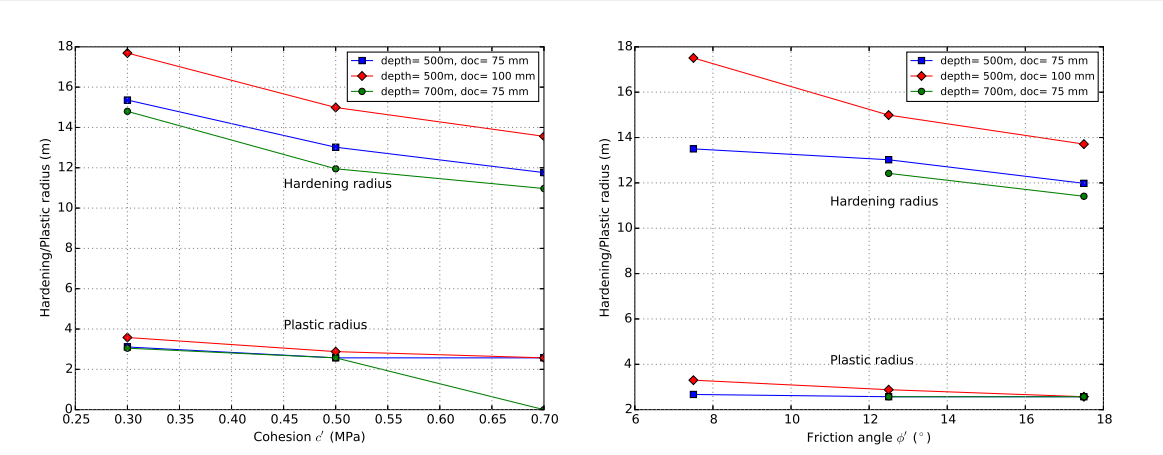

(a) Cohesion c' (b) Friction angle ϕ'

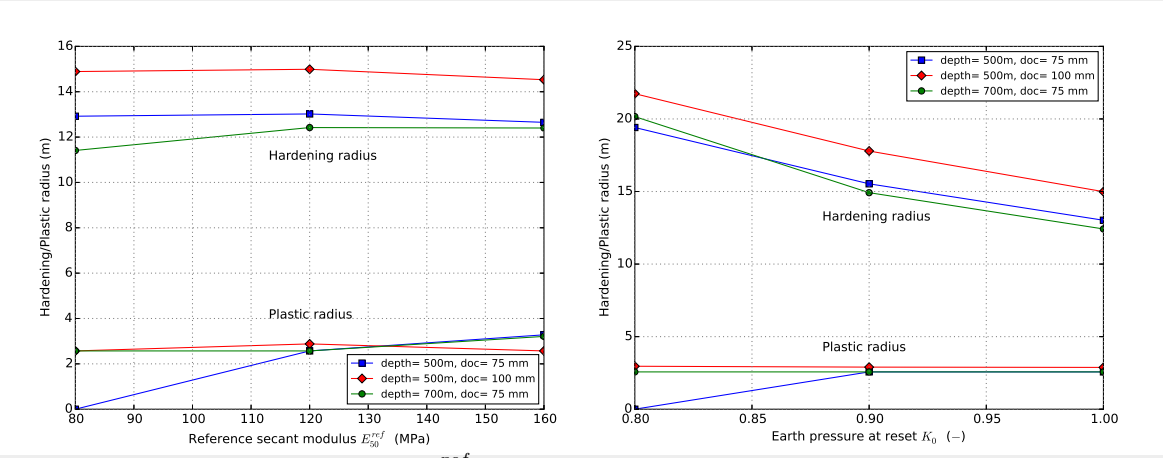

(c) Reference secant modulus E_{50}^{ref} (d) Earth pressure coefficient at rest K_0

Figure 2.10: Extent of the Plastic Zone (PZ) and Hardening Zone (HZ) in the horizontal plane direction of the main gallery for phase (ii): (a,b,c,d) for a variation of the cohesion, c', Friction angle ϕ', Reference secant modulus E_{50}^{ref} and the earth pressure at rest, K_0 for different boundary conditions.

Phase (iii) Tunnel lining opening phase

Figure 2.12 compares the plastic and hardening radii on the cross section 20 m from the tunnel opening, for the variation of the HS model parameters and boundary conditions. It can be seen that the trends in both the plastic and hardening radii in the two phases are similar, compared to the phase (ii), with the removal of the tunnel lining influencing only marginally the extent of the plastic and hardening zones, due to the opening being 20 m away from the evaluated cross section. However, it can be seen that, when the depth is 700 m the hardening zone is more sensitive to the tunnel lining removal.

Phase (iv) Disposal tunnel excavation phase

Figure 2.13 compares the plastic and hardening radii on the cross section 20 m from the tunnel opening of the main gallery in Phase (iv). Compared to the main gallery excavation phase, the extent of the hardening radii moderately increase whereas the plastic radii keep constant for all cases. Again, the largest values are reached for the case of a lower bound cohesion, c', a lower bound friction angle, ϕ' and a lower bound coefficient of earth pressure at rest, K_0. The coefficient of earth pressure at rest, K_0, has the greatest impact and using a value of 0.8 leads to a hardening zone with

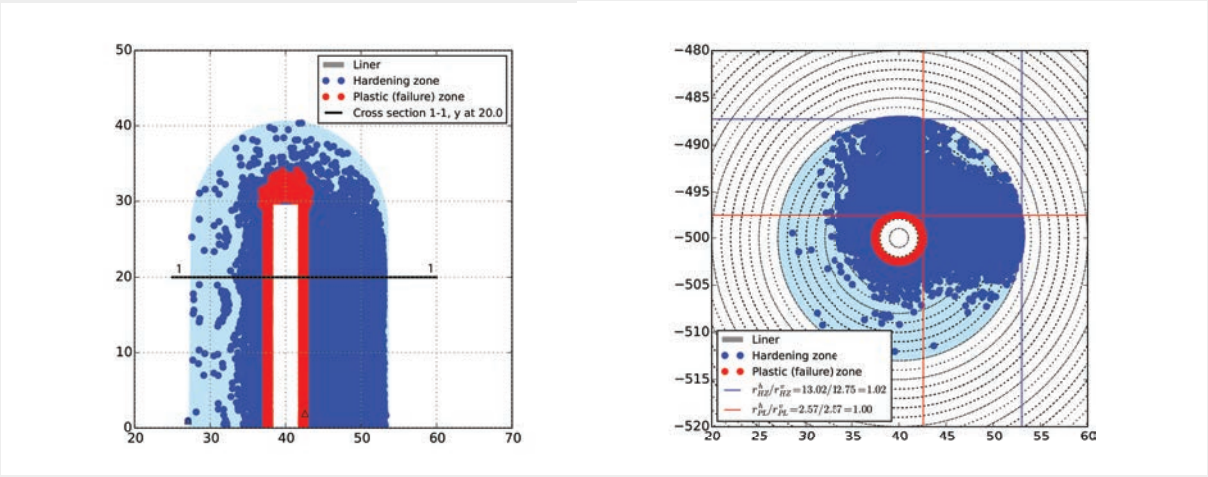

(a) x-y plane $d = 500m$

(b) Earth pressure at rest $K_0 = 1.0$

(c) Earth pressure at rest $K_0 = 0.9$

(d) Earth pressure at rest $K_0 = 0.8$

Figure 2.11: Base case response (with $r_c = 2.4$ m, $d_{oc} = 75$ mm and $d = 500$ m): Gaussian integration points showing the extent of the *Plastic Zone* (PZ) and *Hardening Zone* (HZ): (a) in an isotropic setting ($K_0 = 1$) at $d = 500$ m plane, and (b,c,d) for a variation of the earth pressure at rest, K_0, at $y = 20$ m (1-1 cross section in (a)) plane.

a radius 25 m. The response is again less sensitive to the reference secant modulus, E_{50}^{ref}. However, the lower bound of the reference secant modulus, E_{50}^{ref}, results in the maximum plastic zone for all boundary conditions.

The overcut, once again, has more impact on the hardening and plastic zones than the increase in depth. This means that the construction of the disposal tunnel in these cases will greatly impact the extent of the hardening zone.

Figure 2.14 shows the hardening and plastic radii in the horizontal plane of the disposal (child) tunnel. Similar to the main gallery excavation phase (see Figure 2.10), an increase in the cohesion, c', friction angle, ϕ', and earth pressure coefficient at rest, K_0, results in a decrease in the extent of the hardening zone.

Note that the response of the Boom Clay is anisotropic even if the coefficient of earth pressure at rest is 1 (see Table 2.7), and the ratio of horizontal to vertical extents (r^h/r^v) for both the hardening and plastic zones is around $1.1 - 1.2$. This is because the construction of the main gallery and the tunnel opening cause horizontal stress redistribution around the main gallery, resulting in an anisotropic stresses distribution before the child tunnel excavation. Compared to the Boom Clay response with the undisturbed conditions presented by Arnold et al. (2015), the extents of the plastic

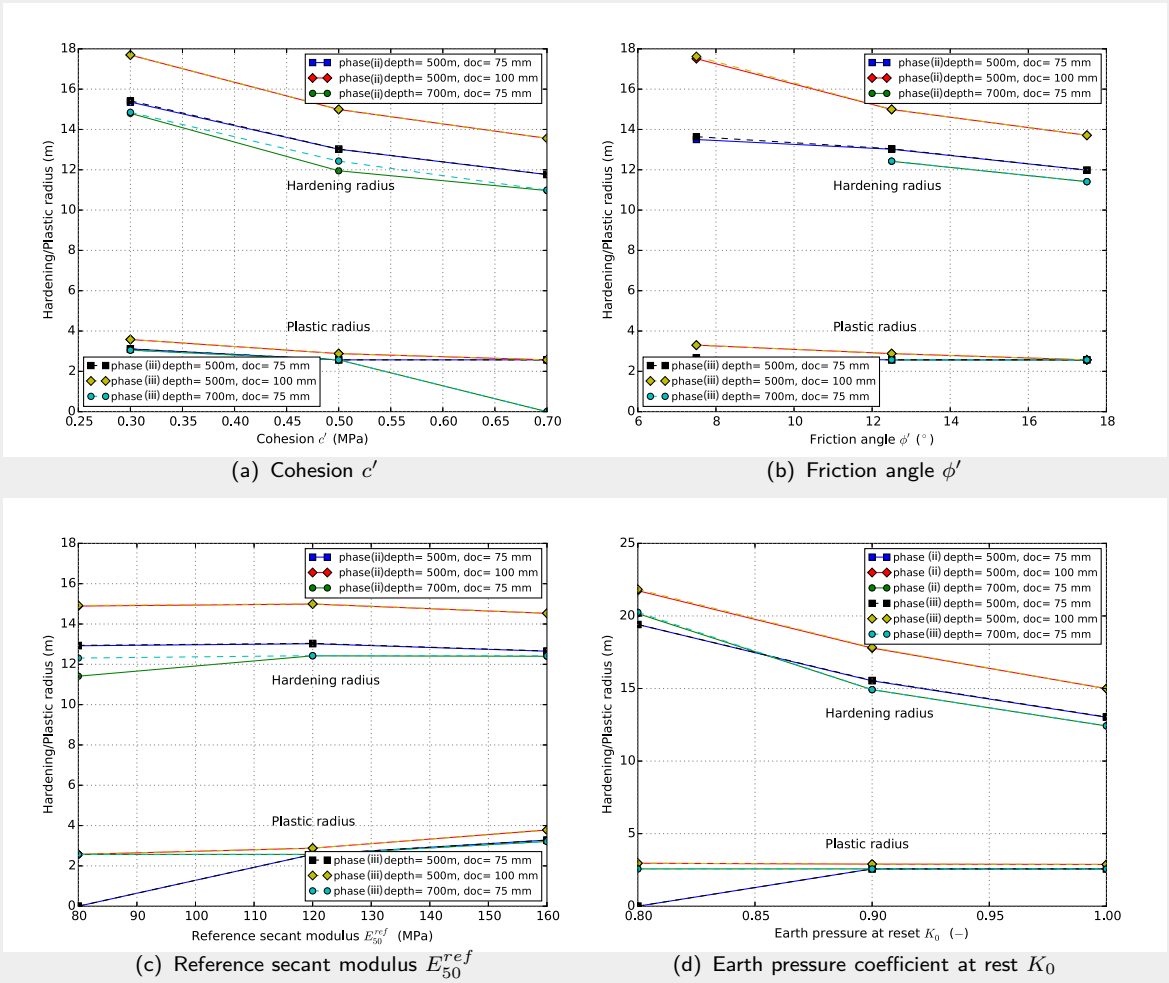

(a) Cohesion c' (b) Friction angle ϕ'

(c) Reference secant modulus E_{50}^{ref} (d) Earth pressure coefficient at rest K_0

Figure 2.12: Comparison of the Plastic Zone (PZ) and Hardening Zone (HZ) in the horizontal plane of the main gallery for phases (ii) and (iii): (a,b,c,d) for a variation of the cohesion, c', Friction angle ϕ', Reference secant modulus E_{50}^{ref} and the earth pressure at rest, K_0, for different boundary conditions.

and hardening zones increase for all cases, which further illustrates that the stress distribution in the surrounding host rock is affected by the main gallery construction and the tunnel lining opening.

Figure 2.15 shows the extents of the hardening and plastic zones for the lower bound of c', ϕ', K_0 and upper bound of E_{50}^{ref} with an overcut $d_{oc} = 100$ mm, for which the largest values of the plastic and hardening zones are reached for these cases. For the cases with lower bound of c', ϕ' and K_0, the range of hardening zones are much larger than compared to that in Figure 2.4(a). In addition, the interaction between the hardening zones where the tunnels cross is significantly increased. This means that when the strength of the host rock is low, or the in situ stress state is anisotropic, the presence of the tunnel crossing will greatly increase the size of the hardening zones around the tunnel crossing area.

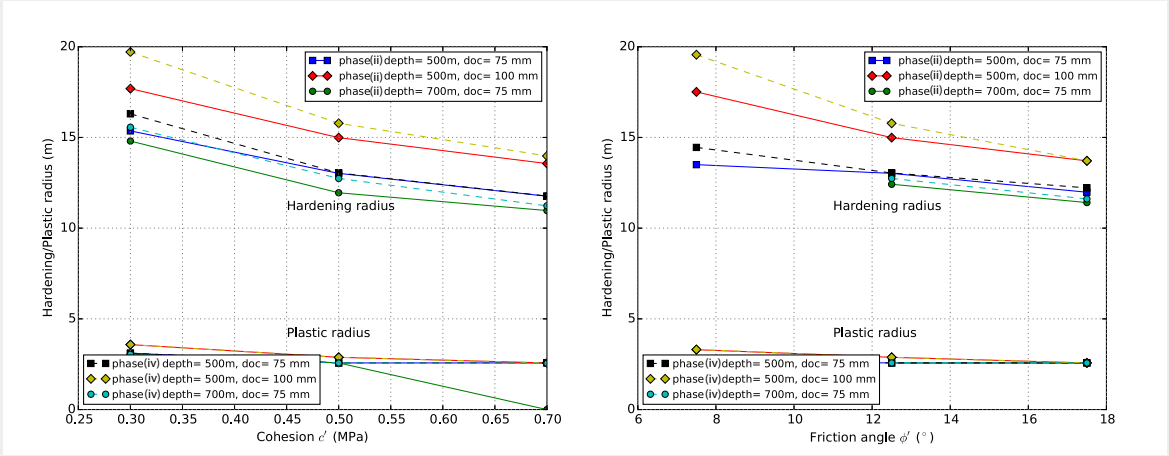

(a) Cohesion c'

(b) Friction angle ϕ'

(c) Reference secant modulus E_{50}^{ref}

(d) Earth pressure coefficient at rest K_0

Figure 2.13: Comparison of the Plastic Zone (PZ) and Hardening Zone (HZ) in the horizontal plane of the main gallery for phases (ii) and (iv): (a,b,c,d) for a variation of the cohesion, c', Friction angle ϕ', Reference secant modulus E_{50}^{ref} and the earth pressure at rest, K_0, for different boundary conditions.

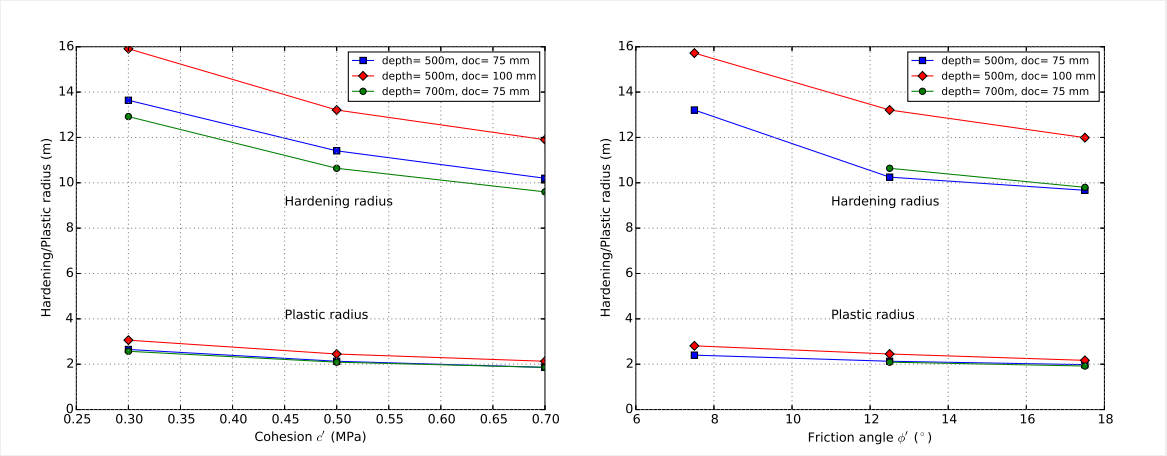

(a) Cohesion c'

(b) Friction angle ϕ'

(c) Reference secant modulus E_{50}^{ref}

(d) Earth pressure coefficient at rest K_0

Figure 2.14: Extent of the Plastic Zone (PZ) and Hardening Zone (HZ) in the horizontal plane of the disposal tunnel: (a,b,c,d) for a variation of the cohesion, c', Friction angle ϕ', Reference secant modulus, E_{50}^{ref}, and the earth pressure at rest, K_0, for different boundary conditions.

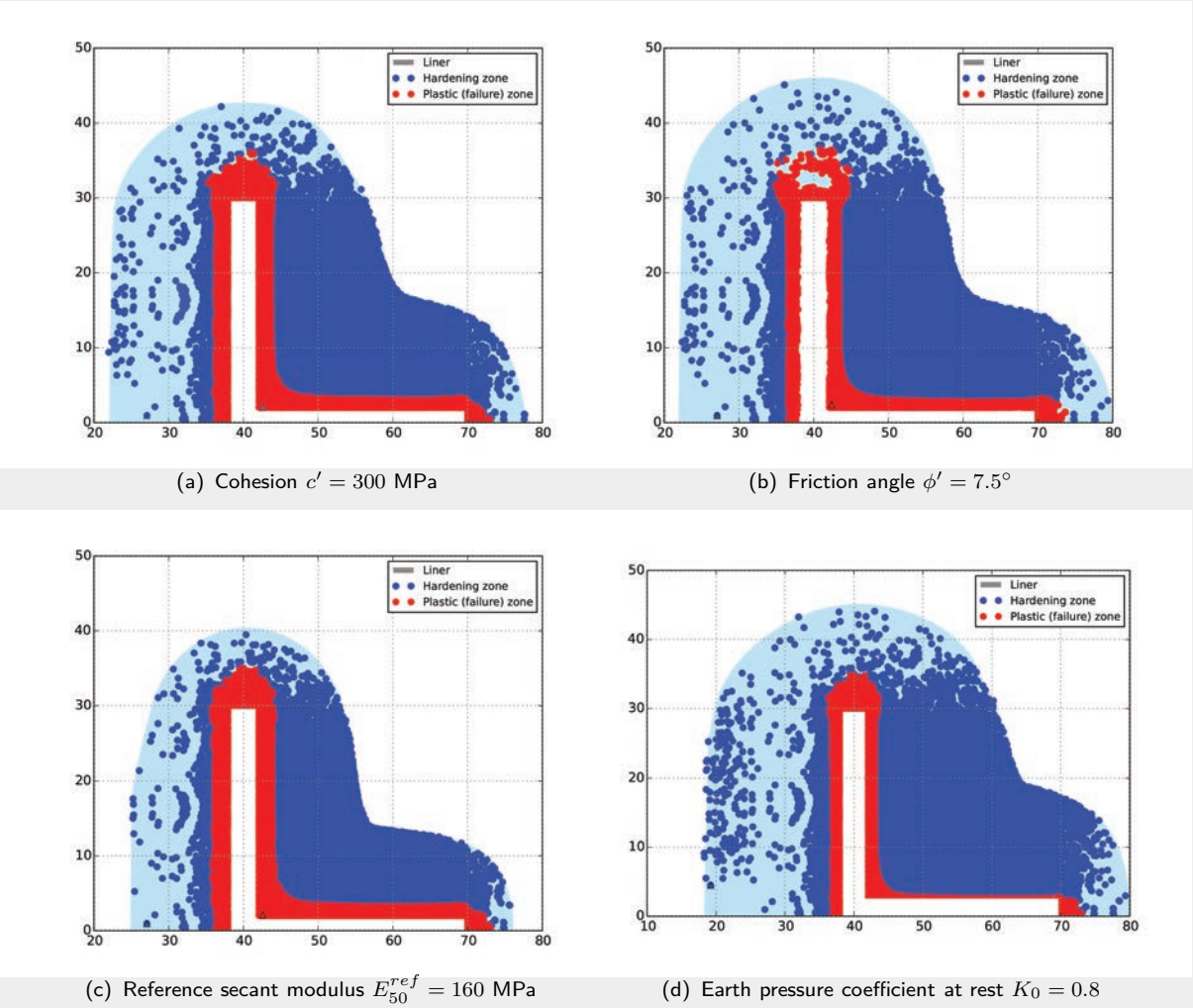

(a) Cohesion $c' = 300$ MPa

(b) Friction angle $\phi' = 7.5°$

(c) Reference secant modulus $E_{50}^{ref} = 160$ MPa

(d) Earth pressure coefficient at rest $K_0 = 0.8$

Figure 2.15: Set-B response (with main gallery $r_c = 2.4$ m, disposal tunnel $r_c = 1.6$ m, $d_{oc} = 100$ mm and $d = 500$ m): Gaussian integration points showing the extent of the *Plastic Zone* (PZ) and *Hardening Zone* (HZ): (a,b,c,d) for lower bound of the cohesion, c', Friction angle ϕ', upper bound of the reference secant modulus E_{50}^{ref} and lower bound of the earth pressure at rest, K_0.

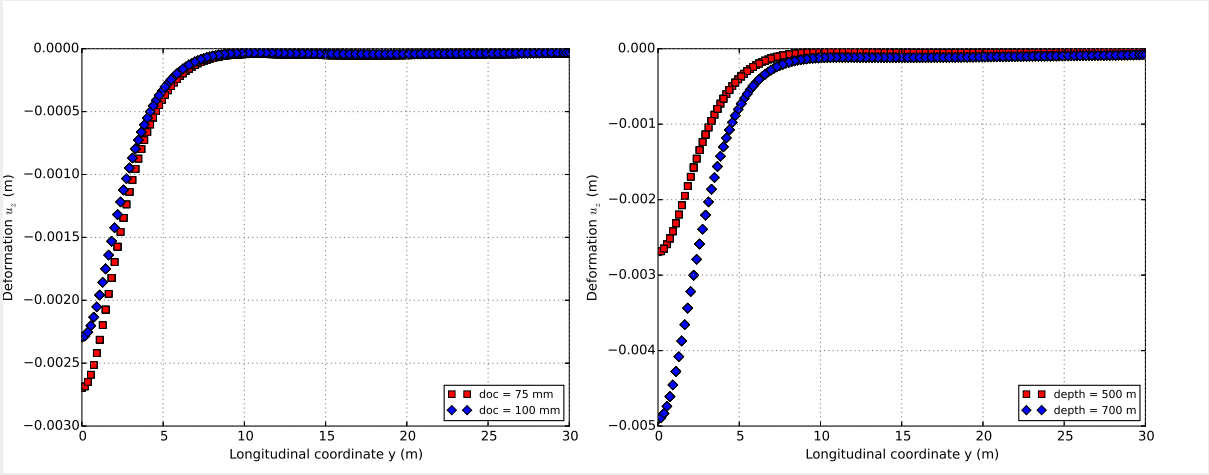

(a) variation of the overcut (b) variation of the depth

Figure 2.16: Vertical deformation u_z along the crown of the main gallery lining: (a) for different overcuts and (b) for different depths.

2.2.2.2 Impact on the lining

The deformation, forces and moments exerted on the lining due to different variations in the model parameters, state variables and boundary conditions are discussed in this section.

In Phase (ii), as shown in Table 2.4, the impact on the moments and forces in the tunnel lining are relatively limited, and are uniform around the tunnel, as shown in Figures 2.7 and 2.8. All the forces are compressive, and within the compressive strength of the material, and all moments are small. These results are similar to those given by Arnold et al. (2015).

The trends with changes in material parameters, state variables and boundary conditions in Phases (iii) and (iv) are similar and therefore only those in Phase (iii) have been detailed.

The majority of the main tunnel deformation occurs during Phase (iii). The displacement along the crown of the main gallery is plotted for various boundary conditions to investigate the deformation response of the tunnel lining due to the tunnel opening. Figure 2.16 shows the main gallery crown vertical deformation along the longitudinal direction. The variations in the deformation for different boundary conditions are similar; they both reach maximum values at the location of the tunnel opening and decrease with increasing distance from the tunnel opening. At around 10 m from the centre of the tunnel opening centre (approximately 2 main tunnel diameters), there is almost no impact. An increase in the overcut d_{oc} reduces the maximum displacement at the crown of the main gallery lining (Figure 2.16 (a)). In contrast, an increase in the depth d significantly increases (almost doubles) the maximum displacement at the crown of the main gallery lining (Figure 2.16 (b)).

Figure 2.17 shows the changes in hoop axial forces with change in model parameters. In all cases, the magnitudes of the absolute minimum hoop forces (compression) are much larger than the absolute maximum hoop forces tension). Furthermore, the maximum hoop forces are fairly insensitive to varying the HS parameters and boundary conditions. An increase in the friction angle and reference secant modulus, ϕ' and E_{50}^{ref}, reduces the absolute value of the minimum hoop forces. In contrast, an increase in cohesion and earth pressure coefficient at rest, c' and K_0, results in a slight increase in the absolute value of the minimum hoop forces. An increase in depth, d, increases the absolute values of the minimum hoop forces significantly.

Figure 2.18 shows the variation of longitudinal moments with parameter variation. It shows that an increase in the friction angle, ϕ', reduces the maximum and minimum longitudinal moments substantially. An increase in the reference secant modulus, E_{50}^{ref}, results in a limited decrease in the maximum and minimum longitudinal moments. It can be seen in Figure 2.18 that the longitudinal moments are rather insensitive to the cohesion and earth pressure coefficient at rest, c' and K_0.

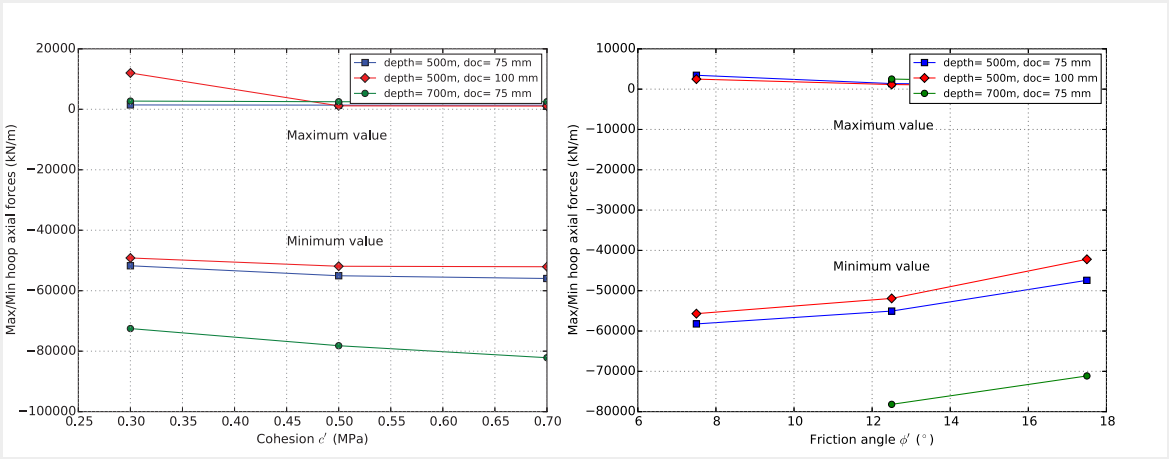

(a) Cohesion c' (b) Friction angle ϕ'

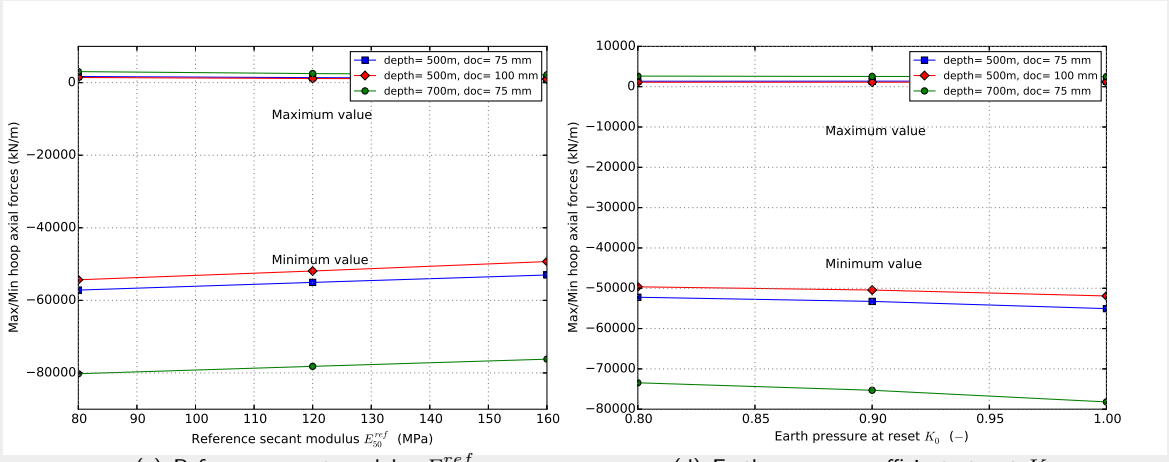

(c) Reference secant modulus E_{50}^{ref} (d) Earth pressure coefficient at rest K_0

Figure 2.17: Hoop axial forces in the lining after main gallery opening (Phase (iii): (a,b,c,d) for a variation of the cohesion, c', Friction angle ϕ', Reference secant modulus E_{50}^{ref} and the earth pressure at rest, K_0, for different boundary conditions.

An increase in depth, d, increases the absolute values of the minimum and maximum longitudinal moments significantly.

The variation in hoop moments is shown in Figure 2.19. As with the longitudinal moments, decreasing the friction angle, ϕ', increases the maximum and minimum hoop moments significantly. Other material properties and the coefficient of earth pressure at rest do not change the moments significantly. As for the previous cases, an increase in the overcut influences only slightly the maximum and minimum hoop moments, but an increase in depth significantly increases the maximum and minimum hoop moments. It is noted that the hoop moment at the springline is significantly larger in all cases than at the crest or invert of the opening.

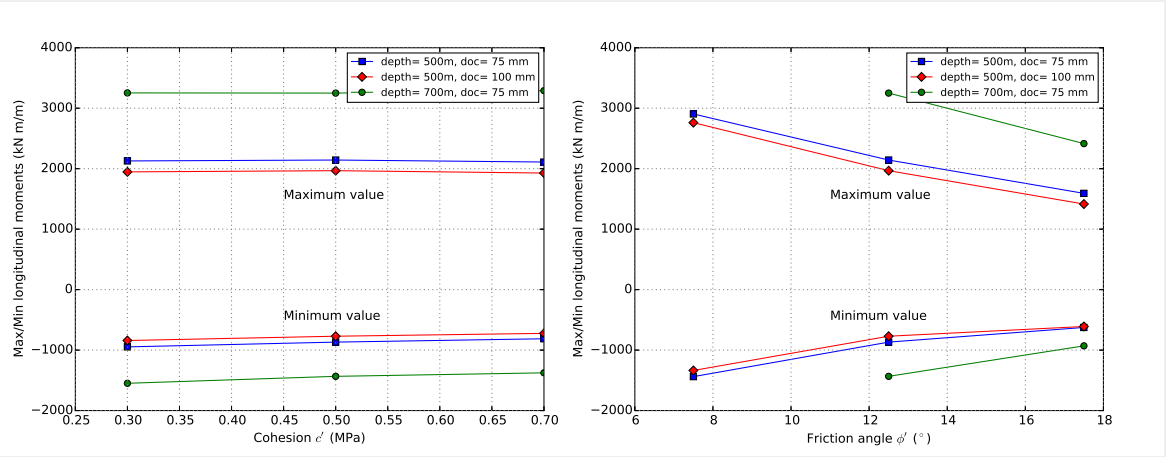

(a) Cohesion c'

(b) Friction angle ϕ'

(c) Reference secant modulus E_{50}^{ref}

(d) Earth pressure coefficient at rest K_0

Figure 2.18: Longitudinal moments in the lining after main gallery opening: (a,b,c,d) for a variation of the cohesion, c', Friction angle ϕ', Reference secant modulus E_{50}^{ref} and the earth pressure at rest, K_0, for different boundary conditions.

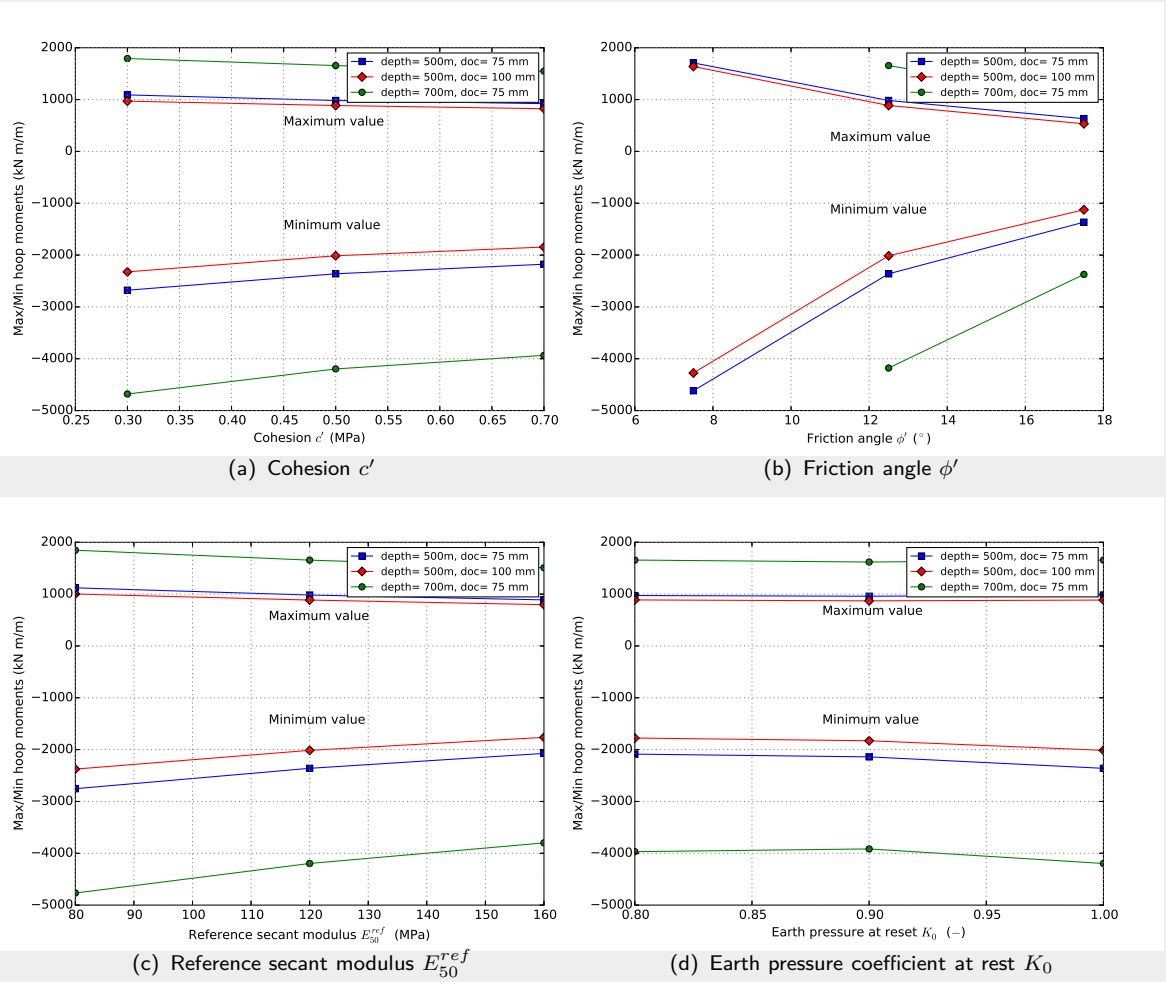

(a) Cohesion c'

(b) Friction angle ϕ'

(c) Reference secant modulus E_{50}^{ref}

(d) Earth pressure coefficient at rest K_0

Figure 2.19: Hoop moments in the lining after main gallery opening: (a,b,c,d) for a variation of the cohesion, c', Friction angle ϕ', Reference secant modulus E_{50}^{ref} and the earth pressure at rest, K_0, for different boundary conditions.

Table 2.8: Summary of the main and disposal gallery responses for Phase (v).

Tunnel	r_{PZ}^{h} * [m]	r_{PZ}^{v} [m]	r_{HZ}^{h} [m]	r_{HZ}^{v} [m]	$N_{1,max}$ [kN/m]	$N_{1,min}$ [kN/m]	$N_{2,max}$ [kN/m]	$N_{2,min}$ [kN/m]	$M_{l1,max}$ [kN m/m]	$M_{l1,min}$ [kN m/m]	$M_{22,max}$ [kN m/m]	$M_{22,min}$ [kN m/m]
Main	2.57	2.57	13.02	12.75	-521.0	-11840	-6858	-37510	1512	-853.0	1313	-1357
Disposal	2.13	2.11	11.41	10.25	801.5	-11390	4083	-22220	1336	-890.4	663.6	-357.0

* Plastic and hardening radii are based on the cross section at y = 20 m (Main) and x=65 m (Disposal).

2.2.3 Set D - local support during excavation

In this section, the analysis undertaken to simulate excavation of the disposal or child tunnel with additional support around the opening is presented. The phases in the simulation follow the approach given in Section 2.1, but to simulate the local support, Phase (iii) was not simulated, i.e. the tunnel lining was left in place during excavation. The local support could take many forms, e.g. a special lining installed at this location or a temporary support in the tunnel close to the opening. An additional phase has been added where this local support was removed, which would only occur if the support was temporary. The sequence of phases then becomes:

(i) a K_0 stage, where the initial vertical and horizontal stresses were calculated (shown in Figure 2.1(b));

(ii) a parent tunnel excavation and construction stage, where the tunnel lining was included and contracted representing rock relaxation (see Figure 2.2(a));

(iii) local support included, simulated via not removing the tunnel lining (see Figure 2.2(b right));

(iv) a child tunnel excavation and construction stage, where the tunnel lining was included and a local rock layer contracted representing rock relaxation (see Figure 2.2(c));

(v) local support removed, simulated via removing the tunnel lining;

The details of the results can be seen in Tables 2.4 - 2.7, and the additional phase, i.e. Phase (v), has been given in Table 2.8.

The results for the behaviour of the Boom Clay, i.e. the plastic and hardening zones are almost identical to the base case results, in that they are governed by the overall impact of the material properties and the overcut, and therefore they are not shown here. The trends in the normal stresses are also similar, but a notable difference is that the child tunnel has higher stresses local to the connection and the main tunnel lower stresses. The major resulting difference in the results is in the moments in the tunnel lining, shown in Figure 2.20, which should be compared with Figure 2.7.

It can be seen that, with permanent local support, i.e. Figure 2.20(c,d), the peak moments at the crown and the invert of the opening are substantially reduced, with the maximum moments in the main tunnel being around 60% of those without local support. If removing the local support, i.e. Phase (v), shown in Figure 2.20(e,f) and numerically in Table 2.8, it can be seen that, compared to the base case (e.g. Figure 2.7), the hoop moments in the main tunnel are approximately 50% of the maximum at the springline and approximately 130% (i.e increase) at the crown. However the overall maximum is reduced and the positive and negative moments are more balanced, which is likely to reduce the amount of reinforcement needed. In the disposal tunnel an increased hoop moment is seen at the springline, as the disposal tunnel forms part of the arch that was formed by the Boom Clay around the main tunnel. This moment, while should be included in the detailed design, is small compared to the maximum moments exhibited in the main tunnel.

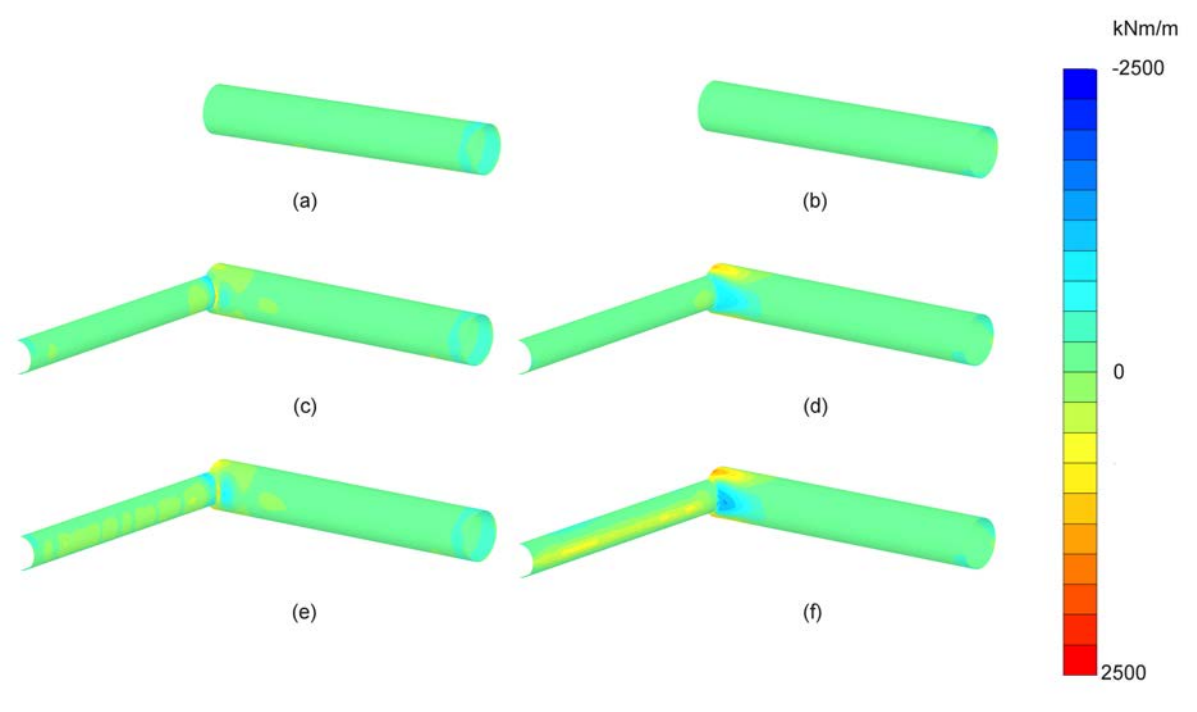

Figure 2.20: Moments acting on the lining per phase for analysis Set D: (a) Phase (ii) longitudual, (b) Phase (ii) hoop, (c) Phase (iv) longitudual, (d) Phase (iv) hoop, (e) Phase (v) longitudual, (f) Phase (v) hoop.

2.3 Design methodologies and constructability

Eurocode 2 (European Committee for Standardisation, 2004) offers methodologies applicable to the design of unreinforced concrete tunnel linings, including the following two fundamental design requirements: (a) compressive stresses in the lining must remain low compared to the concrete design strength, and (b) crack depths must be limited, generally up to 50% of the cross section height for the high axial force load case. The latter requirement is quantified by imposing restrictions on the maximum developing eccentricity $e_{lim} = M/N$ (Kouretzis et al., 2014).

A scoping calculation to understand whether the tunnel construction here is feasible can be undertaken. Unreinforced concrete cannot withstand tension and, moreover, the tunnel lining is likely to be constructed using tunnel lining segments for constructability; therefore, if tension occurs in the tunnel, the lining may separate and be unstable. Limited tension around the tunnel opening can be withstood if local reinforcement is used. Additionally, if the axial force is greater than the compressive strength of the material (e.g. 45 or 80 MPa, depending on the concrete selected), reinforcement, or thickening of the lining would be required.

To calculate tension at the outer edge of the tunnel lining, the combined moment and axial loading must be considered. Figure 2.21 shows the combined effect of the moments and forces on the lining. To determine whether the outer part of the concrete is in tension, the stresses due to the axial load and moment can be summed (e.g. International Tunnelling Association, 2000):

$$\sigma_{outer} = \frac{N}{d} + \frac{|M|y}{I} \tag{2.1}$$

where N is the axial force (tension positive), d is the lining thickness, M is the moment, y is the distance from the outer edge of the lining to the netrual axis of bending and I is the second moment

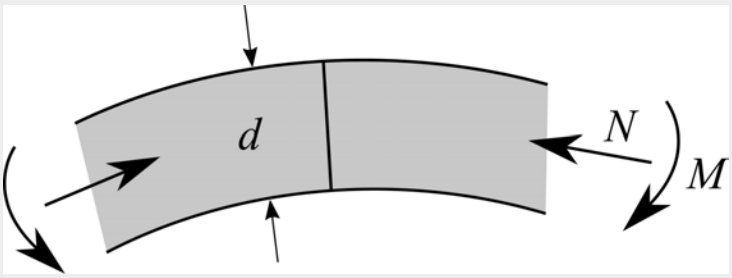

Figure 2.21: Simplified tunnel combined loading.

of inertia. If σ_{outer} is positive, then tension stresses exist and reinforcement is needed. In this case, $I = \frac{bd^3}{12}$, $y = d/2$ and calculating per unit width, gives:

$$\sigma_{outer} = \frac{N}{d} + \frac{6|M|}{d^2} \tag{2.2}$$

The combination of loading should be compatible, i.e. longitudinal moments with longitudinal axial forces and hoop moments with hoop axial forces. For the two tunnel linings, and for the base case scenario, this is plotted in Figures 2.22 for the main gallery lining and 2.23 for the disposal gallery lining. The linings are 'unrolled', i.e. presented flat where the y-axis is along the circumference of the tunnel, and the x-axis is along the tunnel length. In Figure 2.22 the entire circumference is shown, whereas in Figure 2.23 only half the circumference is shown, due to only half the tunnel lining being simulated, due to symmetry.

In can be seen from Figure 2.22(a) that the majority of the tunnel is in compression, as expected, and no tension is apparent, due mainly to the fairly large hoop axial forces. An area of high compressive forces exists, of less than 1 m along the tunnel, around the springline edge of the tunnel opening and additional compressive strength (e.g. reinforcement) would therefore be required here. In Figure 2.22(b) only limited longitudinal stress exists in the majority of the tunnel, and it is therefore easier for tensile stresses to exist. Small areas of tensile stress exist at the tunnel opening crest and invert and a larger area, with smaller stresses, at the edge of the tunnel opening. Tensile reinforcement would be needed here, up to approximately 1 tunnel opening radius away from the opening. From Figure 2.23, no extreme stresses (either tensile or compressive) are generated, and therefore no additional reinforcement is anticipated. At the very edge of the tunnel, at the connection between the tunnels there is a small area of very low compressive stresses, so care should be taken here in detailed design that tension is not developed.

Examining the analysis set D, where local support is provided and then removed, a different reinforcement requirement is observed. Figures 2.24 and 2.25 show the outer edge stress for the main and the child tunnel linings. The more extreme values in the main tunnel are substantially reduced, showing that more moderate reinforcement could be used, but some (relatively low) tension is observed in the hoop direction in the disposal gallery lining. This is due to the Boom Clay arch around the main gallery being partially supported by the disposal gallery lining.

By comparing the behaviour of Set A and Set B (see Section 2.2.2), it is seen that by changing the overcut by only 2.5 cm the hardening zone increases substantially, approximately 20%. This implies that control in the exacvation process is key to controlling damage of the Boom Clay.

The arch formed in the main gallery tunnel lining around the disposal or child tunnel opening provides significant stress re-distribution and, while some reinforcement is needed, this is limited to close to the tunnel opening. This relies on the main gallery being of a larger diameter than the child gallery. For large openings, e.g. between the main and secondary galleries where no arch will occur,

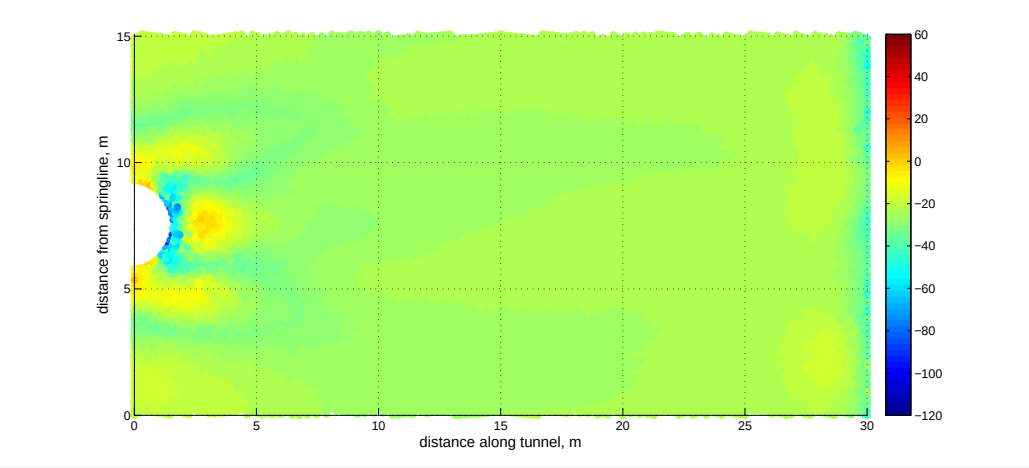

(a) Outer edge hoop stress (MPa) for the main gallery

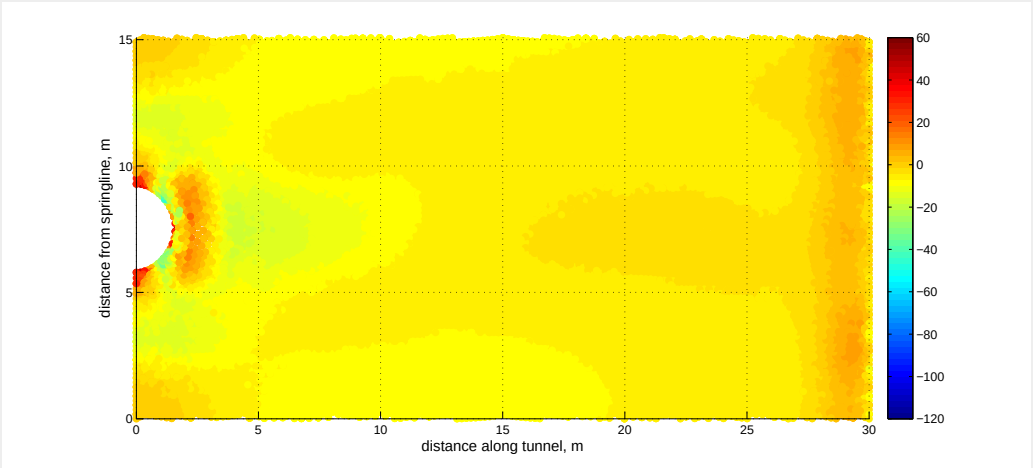

(b) Outer edge axial stress (MPa) for the main gallery

Figure 2.22: Outer edge stress (MPa) of the tunnel lining, where tension is positive, for the main gallery.

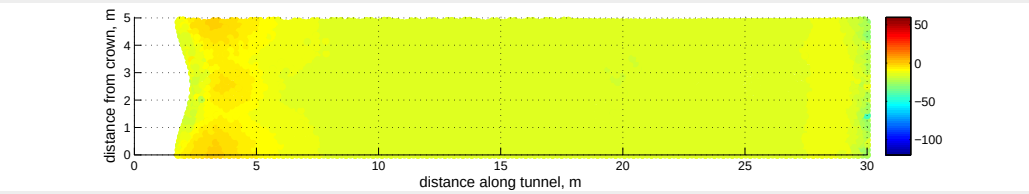

(a) Outer edge hoop stress (MPa) for the disposal gallery

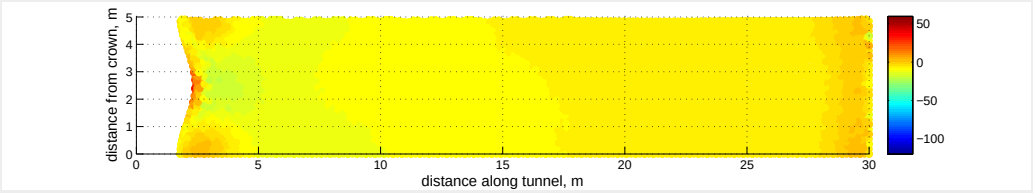

(b) Outer edge axial stress (MPa) for the disposal gallery

Figure 2.23: Outer edge stress (MPa) of the tunnel lining, where tension is positive, for the disposal gallery. Half the tunnel is shown due to symmetry

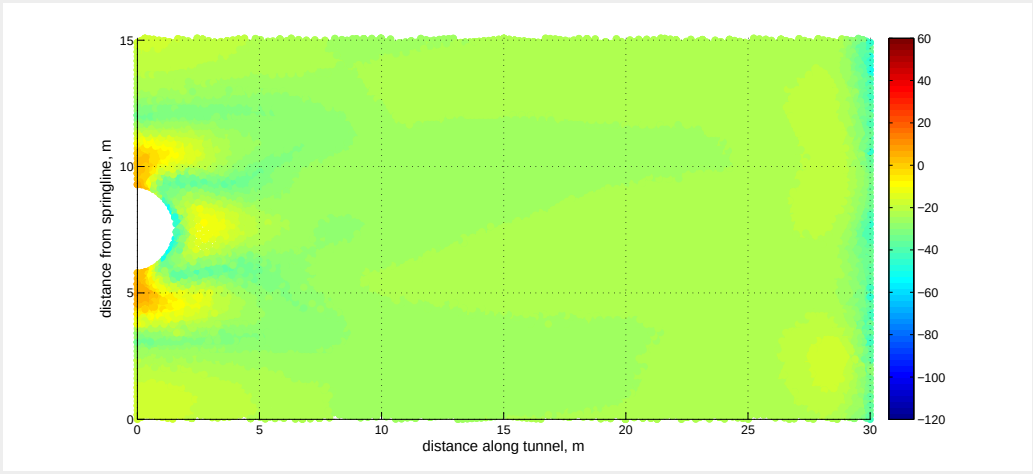

(a) Outer edge hoop stress (MPa) for the main gallery

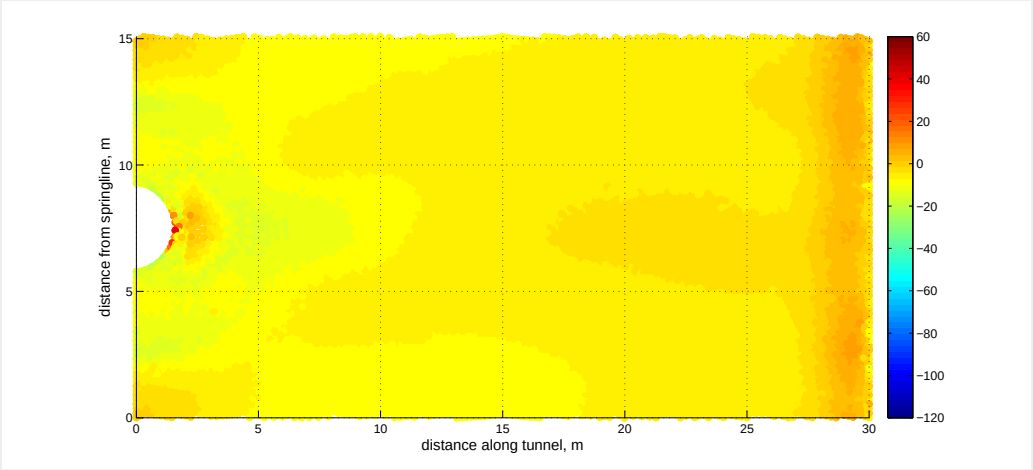

(b) Outer edge axial stress (MPa) for the main gallery

Figure 2.24: Outer edge stress (MPa) of the tunnel lining, where tension is positive, for the main gallery, where local support is provided and then removed (Analysis set D, Phase (v)).

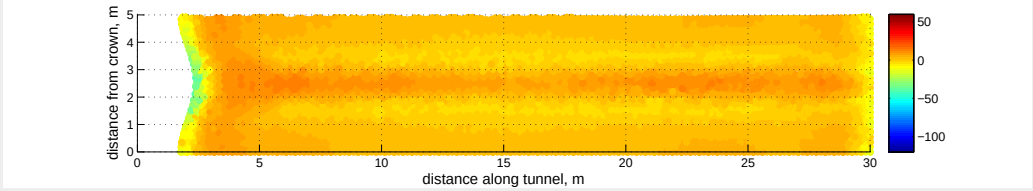

(a) Outer edge hoop stress (MPa) for the disposal gallery

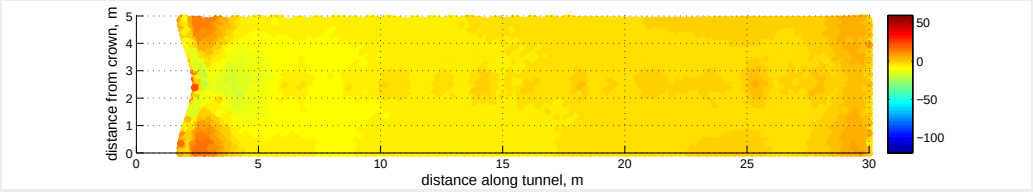

(b) Outer edge axial stress (MPa) for the disposal gallery

Figure 2.25: Outer edge stress (MPa) of the tunnel lining, where tension is positive, for the disposal gallery, where local support is provided and then removed (Analysis set D, Phase (v)). Half the tunnel is shown due to symmetry

more substantial additional support will be needed. Constructing two ajoining tunnels of the same diameter with a tunnel boring machine would typically require a large starting chamber (of greater diameter) and is therefore unlikely to be suitable here. Moreover, a tunnel boring machine would need to be able to manoevered inside the main gallery and having both tunnels of the same diameter would require an innovative tunnel boring machine, which would be able to be constructed in situ and of a shorter length than diameter. It is also noted that it may be more practical to allow the tunnel boring machine to either be able to be removed from the tunnel in pieces or to tunnel through to another gallery. In these cases the tunnel boring machine could then be reuseable.

3 Conclusions and recommendations

This report has presented an investigation of the response of the Boom Clay and tunnel lining due to a lateral opening of a main tunnel and construction of waste disposal gallery. Three dimensional numerical modelling was used and a calibrated constitutive model (the HS model) was used. A mechanical sensitivity analysis was performed by varying the critical HS model parameters, the in situ stress states and the boundary conditions simulating the tunnel crossings in an undrained analysis. Special attention was given to the extent of the hardening and plastic zones at the each construction phase, as well as the deformation distributions and the internal forces and moments in the tunnel lining during the tunnel lateral opening phase.

It was seen that, in the base case results based on the most likely set of parameters, the construction of the disposal tunnel had only a limited impact on the damaged (plastic and hardening) zone around the tunnel. However, the tunnel lining was subjected to significantly increased moments and forces locally due to the tunnel opening. It was shown that only limited areas, surrounding the tunnel openings, should be reinforced (limited to approximately 1 tunnel opening radius away from the opening).

The sensitivity analysis showed that the friction angle is, as also reported by Arnold et al. (2015), an important parameter controlling the development of the damaged zone, as is the stress state anisotropy in the clay. For low shear strengths and highly anisotropic stress conditions the damaged zone of the clay expanded substantially away from both the main and disposal tunnels, creating an expanded damaged zone. The overcut was seen to be more important than the depth in controlling the damaged zones, although increasing both increased the moment developed on the lining.

By adding local support around the tunnel opening during the excavation, a reduction in the maximum moments and forces could be seen, which will allow a reduction in the permanent reinforcement needed. However, local support was not found to be essential.

In the cases presented here, the disposal tunnel was of a smaller diameter than the gallery. It is recommended that for constructability purposes this is the case for the disposal galleries, due to the stress redistriution in the tunnel lining and the practical use of a tunnel boring machine.

The results in this report are presented with respect to the objective of technical feasibility. Detailed design should be undertaken prior to construction.

References

Arnold, P., P. J. Vardon, M. A. Hicks, J. Fokkens and P. A. Fokker (2015). *A numerical and reliability-based investigation into the technical feasibility of a Dutch radioactive waste repository in Boom Clay*. OPERA-PU-TUD311. Centrale Organisatie Voor Radioactief Afval (COVRA N.V.)

Biliris, C. and A. Purwodihardjo (2005). Numerical analysis of an opening in a bolted cast iron tunnel lining. In: *Proceedings of Underground Construction 2005*.

European Committee for Standardisation (2004). *Eurocode 2: Design of Concrete Structures: Part 1: General Rules and Rules for Buildings*. EN 1992-1-1 :2004. European Committee for Standardization.

Hafez, N. M. (1995). *Post-failure modelling of three-dimensional shotcrete lining for tunelling*. na.

Hoek, E. and E. T. Brown (1980). Underground excavations in rock. In: *Underground Excavations in Rock*, 527.

Hsiao, F. Y., C. L. Wang and J. C. Chern (2009). Numerical simulation of rock deformation for support design in tunnel intersection area. In: *Tunnelling and Underground Space Technology* 24 (1), 14–21. DOI: 10.1016/j.tust.2008.01.003.

International Tunnelling Association (2000). Analysis of circular tunnels due to seismic P-wave propagation, with emphasis on unreinforced concrete liners. In: *Tunnelling and Underground Space Technology* 15 (3), 303 –331.

Jäger, J. (2002). Tunnel junction at shallow cover: a case study. In: *Proceedings of the third international conference on Engineering computational technology*. Civil-Comp press, pp. 61–62.

Jones, B. (2007). Stresses in sprayed concrete tunnel junctions. PhD thesis. University of Southampton.

Kouretzis, G. P., K. I. Andrianopoulos, S. W. Sloan and J. P. Carter (2014). Analysis of circular tunnels due to seismic P-wave propagation, with emphasis on unreinforced concrete liners. In: *Computers and Geotechnics* 55, 187 –194.

Li, Y., X. Jin, Z. Lv, J. Dong and J. Guo (2016). Deformation and mechanical characteristics of tunnel lining in tunnel intersection between subway station tunnel and construction tunnel. In: *Tunnelling and Underground Space Technology* 56, 22 –33.

Moon, H. and H. Lee (1991). A 3-D FE model of a shaft-tunnel-tunnel intersection and comparison with a 2-D model. In: *International Society for Rock Mechanics - 7th ISRM Congress*.

Pant, B. (1971). Analysis and design of pressure tunnel intersection. In: *Indian Society of Engineering Geology, Tunnelling Seminar, Part I*.

Plaxis (2015). *PLAXIS 3D Anniversary Edition - Reference Manual*. Delft, The Netherlands: Plaxis bv.

Ren, G., J. V. Smith, J. W. Tang and Y. M. Xie (2005). Underground excavation shape optimization using an evolutionary procedure. In: *Computers and Geotechnics* 32 (2), 122–132.

Riley, W. (1964). Stresses at tunnel intersections. In: *J. Eng. Mech. Div. Proc. ASCE* 90, 167–179.

Schanz, T. (1998). Zur Modellierung des mechanischen Verhaltens von Reibungsmaterialien. PhD thesis. Stuttgart, Germany: Mitteilung 45, Institut für Geotechnik, Universität Stuttgart, Universität Stuttgart.

Schanz, T., P. A. Vermeer and P. G. Bonnier (1999). The Hardening Soil model – formulation and verification. In: *Proceedings Plaxis Symposium "Beyond 2000 in Computational Geotechnics"*. Amsterdam: Balkema, pp. 281–296.

Spyridis, P. and K. Bergmeister (2015). Analysis of lateral openings in tunnel linings. In: *Tunnelling and Underground Space Technology* 50, 376–395. DOI: 10.1016/j.tust.2015.08.005.

Takino, K., H. Kimura, N. Takeda and F. Ito (1985). Three-dimensional behaviour of tunnel intersection. In: *International conference on numerical methods in geomechanics*, pp. 1185–1192.

Thareja, D. V., K. Madhavan, K. G. Sharma and R. Natarajan (1985). Three dimensional finite element analysis of branching tunnels. In: *International conference on numerical methods in geomechanics*, pp. 1193–1199.

— (1997). Recent developments and application of the boundary element method in geomechanics. In: *Numerical models in geomechanics*, pp. 461–467.

Tsuchiyama, S., M. Hayakawa, T. Shinokawa and H. Konno (1988). Deformation behaviour of the tunnel under the excavation of crossing tunnel. In: *Proc. 6th Int. Conf. on Numerical Methods in Geomechanics*, 1591–1596.

Van Cotthem, A., H. Van Humbeeck and E. Biurrun (2012). Underground Architecture and Layout for the Belgian High-Level and Long-Lived Intermediate-Level Radioactive Waste Disposal Facility-12116. In: *Proceedings of the WM2012 Conference*.

Verhoef, E., E. Neeft, J. Grupa and A. Poley (2014). *Outline of a disposal concept in clay, OPERA-PG-COV008, First update*. Centrale Organisatie Voor Radioactief Afval (COVRA N.V.) URL: http://www.covra.nl/cms-file/get/iFileId/2813.

Young, W. C. (1989). Roark's formulas for stress and strain. In: *McGraw Hi11 Book Company, New York*.

OPERA

Meer informatie:

Postadres
Postbus 202
4380 AE Vlissingen

T 0113-616 666
F 0113-616 650
E info@covra.nl

www.covra.nl